1 **Cysteine depletion triggers adipose tissue thermogenesis and weight-loss.**
2
3 Aileen H. Lee[1,2,3*], Lucie Orliaguet[1,2,3*], Yun-Hee Youm[1,2,3], Rae Maeda[4], Tamara Dlugos[1,2,3],
4 Yuanjiu Lei[1,2,3], Daniel Coman[5,6], Irina Shchukina[7], Sairam Andhey[7], Steven R. Smith[8], Eric
5 Ravussin[9], Krisztian Stadler[9], Fahmeed Hyder[5,6], Maxim N. Artyomov[7], Yuki Sugiura[4] and
6 Vishwa Deep Dixit[1,2,3,10]
7
8
9 [1]Department of Pathology, [2]Department of Comparative Medicine, [3]Department of
10 Immunobiology, Yale School of Medicine, New Haven, CT 06520, USA. [4] University of Kyoto,
11 Japan, [5]Department of Radiology and Biomedical Imaging, [6]Department of Biomedical
12 Engineering, School of Engineering and Applied Science, Yale University. [7]Department of
13 Pathology and Immunology Washington University School of Medicine, St. Louis, MO 63110,
14 USA. [8]Translational Research Institute for Metabolism and Diabetes, AdventHealth, Orlando, FL,
15 USA. [9]Pennington Biomedical Research Center, Baton Rouge, LA, USA., [10]Yale Center for
16 Research on Aging, Yale School of Medicine, New Haven, CT 06520, USA
17
18 *Co-first authors

19 Lead Contact: Vishwa Deep Dixit,
20 Yale School of Medicine
21 310 Cedar St, New Haven CT 06520
22 Email: Vishwa.Dixit@yale.edu
23 Phone: 203-785-2525
24 Fax: 203-785-7499
25

26

Abstract

28   Dietary interventions such as caloric restriction (CR)[1] and methionine restriction[2] that prolong

29   lifespan induce the 'browning' of white adipose tissue (WAT), an adaptive metabolic response

30   that increases heat production to maintain health[3,4]. However, how diet influences adipose

31   browning and metabolic health is unclear. Here, we identified that weight-loss induced by CR in

32   humans[5] reduces cysteine concentration in WAT suggesting depletion of this amino-acid may be

33   involved in metabolic benefits of CR. To investigate the role of cysteine on organismal

34   metabolism, we created a cysteine-deficiency mouse model in which dietary cysteine was

35   eliminated and cystathionine γ-lyase (CTH)[6], the enzyme that synthesizes cysteine was

36   conditionally deleted. Using this animal model, we found that systemic cysteine-depletion causes

37   drastic weight-loss with increased fat utilization and browning of adipose tissue. The restoration

38   of dietary cysteine in cysteine-deficient mice rescued weight loss together with reversal of adipose

39   browning and increased food-intake in an on-demand fashion. Mechanistically, cysteine

40   deficiency induced browning and weight loss is dependent on sympathetic nervous system derived

41   noradrenaline signaling via β3-adrenergic-receptors and does not require UCP1. Therapeutically,

42   in high-fat diet fed obese mice, one week of cysteine-deficiency caused 30% weight-loss and

43   reversed inflammation. These findings thus establish that cysteine is essential for organismal

44   metabolism as removal of cysteine in the host triggers adipose browning and rapid weight loss.

50   **Main**

51   The Comprehensive Assessment of Long-term Effects of Reducing Intake of Energy (CALERIE-

52   II) clinical trial in healthy adults demonstrated that a simple 14% reduction of calories for two

53   years without any specific dietary prescription to alter macronutrient intake or meal timings can

54   reprogram the immunometabolic axis to promote healthspan[5,7,8]. Harnessing the pathways engaged

55   by CR in humans may expand the current armament of therapeutics against metabolic and immune

56   dysfunction. Induction of negative energy balance and resultant activation of mitochondrial fatty

57   acid oxidation by CR is thought to underlie some of its beneficial effects on healthspan[5]. However,

58   it has also been suggested that CR-induced metabolic effects may be due to decreased protein

59   intake in food-restricted animal models[9,10]. Adding back individual amino acids to calorie-

60   restricted *Drosophila* abolished the longevity effects, and traced to the limitation of methionine,

61   an important node for lifespan extension[10]. Indeed, methionine restriction (MR) in rodents

62   increases lifespan[11] with enhanced insulin sensitivity, adipose tissue thermogenesis, and

63   mitochondrial fatty acid oxidation[2]. Surprisingly, in long-lived *Drosophila* fed an MR diet, adding

64   back methionine did not rescue the pro-longevity effect of diet, and it was hypothesized that

65   activation of the methionine cycle may impact longevity[10]. Commercial MR diets contain 0.17%

66   methionine compared to normal levels of 0.86%, but notably, the MR diets also lack cystine[12, 13],

67   another sulfur-containing amino acid (SAA), which is a key substrate for protein synthesis,

68   including synthesis of glutathione, taurine and iron-sulfur clusters[6,14]. Interestingly, in rats, MR-

69   induced anti-adiposity and pro-metabolic effects, including reduction of leptin, insulin, IGF1, and

70   elevation of adiponectin, were reversed when animals were supplemented with cysteine in the

71   diet[15]. Furthermore, cysteine supplementation in MR rats did not restore low methionine,

72   suggesting no increase in the methionine cycle[15], where homocysteine is converted into methionine

73 via the enzyme betaine-homocysteine S-methyltransferase (BHMT)[6]. The existence of

74 transsulfuration (TSP) in mammals indicates that in case of dietary cysteine scarcity, the host

75 shuttles homocysteine from the methionine cycle via the production of cystathionine, which is then

76 hydrolyzed into cysteine by the enzyme cystathionine γ-lyase (CTH)[6,16]. Cysteine is an ancient

77 molecule that evolved to allow early life to transition from anoxic hydrothermal vents into

78 oxidizing cooler environment[17,18]. Thus, cysteine, the only thiol-containing proteinogenic amino

79 acid, is essential for disulfide bond formation, and redox signaling, including nucleophilic

80 catalysis[6,16]. It remains unclear if cysteine specifically controls organismal metabolism and

81 whether sustained CR in healthy humans can help understand the fundamental relationship

82 between energy balance and sulfur-containing amino acid homeostasis pathways that converge to

83 improve healthspan and lifespan.

84

85 **CR in humans reduces adipose tissue cysteine.**

86 Adipose tissue regulates organismal metabolism by orchestrating inter-organ communication

87 required for healthy longevity. To study the mechanisms that drive CR's beneficial effects on

88 human metabolism, we conducted an unbiased metabolomics analysis of the subcutaneous adipose

89 tissue (SFAT) of participants in the CALERIE-II trial at baseline and one year after 15% achieved

90 CR and weight loss[5,7, 8]. The PLSDA analyses of abdominal SFAT biopsies revealed that one year

91 of mild sustained CR significantly altered the adipose tissue metabolome (Fig. 1a). The unbiased

92 metabolite sets enrichment analyses demonstrated significant increases in cysteine, methionine,

93 and taurine metabolism, which indicates rewiring of cysteine metabolism that involves

94 transsulfuration pathway (TSP) (Fig. 1b, c). To investigate the role of TSP in human CR, we re-

95 analyzed our previously reported RNA sequencing data of humans that underwent CR[5,7]. These

96   analyses revealed that compared to baseline, one and two years of CR in humans increased the

97   adipose expression of *CTH* (Fig. 1d) with a concomitant reduction in the expression of *BHMT*

98   (Fig. 1e) suggesting reduction in methionine cycle and shift towards TSP (Fig. 1c). Interestingly,

99   prior studies have found that long-lived rodents upregulate metabolites in TSP that generates

100   cysteine from methionine[19,20]. Consistent with our findings in human CR, data from multiple

101   lifespan-extending interventions in rodents identified upregulation of CTH as a common signature

102   or potential biomarker of longevity[21].

103   Metabolomic analyses revealed that despite an increase in *CTH* expression post-CR,

104   adipose cysteine levels were significantly reduced upon CR (Fig. 1f) with no change in

105   homocysteine and cystathionine (Extended Data Fig 1a). Consistent with the reduced expression

106   of *BHMT*, there was a decline in concentration of dimethylglycine (DMG) (Fig. 1f). CR caused a

107   reduction in cysteine derived metabolites, γ-glutamyl-cysteine (γ-Glu-Cys), glutathione (GSH),

108   and cysteinylglycine (Cys-Gly) (Fig. 1g). Collectively, these results suggests that CR in humans

109   reduces enzymes and metabolites that feed into methionine cycle and lowers cysteine (Fig. 1c).

110 Cysteine depletion causes lethal weight loss in mice.

111   Cysteine is thought to be biochemically irreplaceable because methionine, the other sole

112   proteinogenic SAA, lacks a thiol group and hence cannot form complexes with metals to control

113   redox chemistry[22]. To determine whether cysteine is required for survival and organismal

114   metabolism, we created a loss of function model where cysteine becomes an essential amino acid

115   requiring acquisition from the diet by deletion of CTH (*Cth*^{-/-} mice) (Fig. 1h and Extended data

116   Fig. 1b). Cysteine deficiency was thus induced by feeding adult *Cth*^{-/-} mice a custom amino acid

117   diet that only lacks cystine (CysF diet), while control mice were fed an isocaloric diet that

118   contained cystine (CTRL diet) (Fig. 1h). Utilizing this model, we found that mice with cysteine

119   deficiency rapidly lost ~25-30% body weight within 1 week compared to littermate $Cth^{+/+}$ mice

120   fed a CysF diet or $Cth^{-/-}$ fed a control diet (Fig. 1i, Extended data Fig. 1b). Upon clinical

121   examination of the cysteine deficient mice, 30% weight loss is considered a moribund state that

122   required euthanasia. The weight loss in mice lacking CTH and cystine in the diet was associated

123   with significant fat mass loss relative to lean mass (Extended data Fig. 1c) in cysteine-deficient

124   animals. Pair feeding of cysteine-replete mice with cysteine depleted diet fed animals produced

125   similar weight-loss (Extended data Fig. 1e). This rapid weight loss is not due to malaise or

126   behavioral alteration, as $Cth^{-/-}$CysF mice displayed normal activity and a slight reduction in food

127   intake in the first 2 days after CysF diet switch that was not significantly different (Extended data

128   Fig. 1f and link of video file of cage activity). The Cth deficient mice on the control diet were

129   indistinguishable from control littermates in parameters indicative of health, they displayed higher

130   nest building and no change in grip strength, gait, ledge test, hindlimb clasping, and displayed no

131   clinical kyphosis (Extended data Fig. 1g, h). Furthermore, compared to $Cth^{-/-}$ mice on control diet,

132   the analyses of liver, heart, lungs, and kidneys of $Cth^{-/-}$CysF mice did not reveal pathological

133   lesions indicative of tissue dysfunction (Extended data Fig. 1i). Notably, restoration of up to 75%

134   cysteine levels in the diet of $Cth^{-/-}$ CysF mice that were undergoing weight-loss was sufficient to

135   completely rescue the body weight over three weight-loss cysteine depletion cycles, demonstrating

136   the specificity and essentiality of cysteine for the organism (Fig. 1j).

137   To identify systemic changes in metabolites upon cysteine deficiency, we conducted serum

138   and adipose tissue metabolomics analyses. Compared to Cth-deficient mice fed a normal diet, the

139    $Cth^{-/-}$CysF mice had reduced cystine levels, suggesting that cysteine deficiency is maintained by a

140   reduction in systemic cystine levels (Fig. 1k). Cysteine depletion also elevated the cystathionine

141   and L-serine levels, compared to control diet fed animals (Fig. 1k). Other sulfur amino acid (SAA)

142   metabolites such as methionine, homocysteine (HCys) and glutamic acid were not significantly

143   changed (Extended data Fig. 1j). Taurine levels in the Cth deficient mice on cysteine free diet also

144   did not change compared to control animals (data not shown). Interestingly, the gamma-glutamyl

145   peptide analogs of cysteine and GSH such as 2-aminobutyric acid (2AB) and ophthalmic acid (OA

146   or γglutamyl-2AminobutyrylGlycine) were increased in the serum of cysteine deficient mice (Fig.

147   1k). Notably, in subcutaneous adipose tissue, cysteine deficiency did not affect glutathione (GSH)

148   (Extended data Fig. 1k) but lowered oxidized GSH (GSSG) concentration, a key downstream

149   product derived from cysteine in TSP (Fig. 1l, m). The increase in γ-glutamyl peptides (2AB and

150   OA) in cysteine-limiting conditions *in vivo* is consistent with studies that show that GCLC can

151   synthesize γglutamyl-2AminobutyrylGlycine in a GSH independent manner and prevents

152   ferroptosis by lowering glutamate generated oxidative stress[23]. OA is a GSH analog in which the

153   cysteine group is replaced by L-2-aminobutyrate (2AB). 2oxobutyrate is the canonical substrate

154   for 2AB in cysteine-replete conditions such that 2AB is produced from 2OB and glutamate in the

155   presence of aminotransferases[24]. Thus, the increase in 2AB despite the removal of cysteine in diet

156   could be due to an alternative pathway of deamination of threonine into 2AB[25]. Indeed, L-

157   threonine levels are increased upon cysteine depletion in mice (Fig. 1m). Prior studies found that

158   GSH can inhibit glutamate cysteine ligase (GCLC)[26,27] regulating its production by a feedback

159   mechanism. Thus, the removal of cysteine and reduction of GSH may release this disinhibition

160   (Fig 1l). Consistent with this hypothesis and elevated OA levels, *Gclc* and *Gss* expression were

161   increased in cysteine-starved mice (Fig. 1n). The increased OA production vs GSH production

162   reveals adaptive changes induced by systemic cysteine deficiency. Cysteine is also required for

163   Fe-S clusters in numerous proteins[18,28]. We found that cystine-depletion upregulates *Bola3* (Fig.

164   1o) and *Isca1* gene expression in adipose tissue without affecting *Nfs1* (Extended data Fig. 1l),

165   which are implicated in FeS cluster formation[28]. Consistent with the association between increased

166   *Bola3* and adipose browning in a cysteine-deficient state, adipose-specific deletion of *Bola3*

167   decreases EE and increases adiposity in mice upon aging[29]. The impact of cysteine starvation on

168   Fe-S cluster formation and function requires further studies. The *in vivo* spin trapping and electron

169   paramagnetic resonance (EPR) spectroscopy revealed that cysteine deficiency significantly

170   increased lipid-derived radicals in BAT with undetectable signals in WAT (Fig 1p, Extended Data

171   1m). Also, given aconitase is regulated by reversible oxidation of $(4Fe-4S)^{2+}$ and cysteine residues,

172   depletion of cysteine also reduced aconitase activity in SFAT with no change in BAT (Fig1q).

173   Together, these data demonstrate that removing cysteine causes lethal weight loss and induces

174   adaptive changes in organismal metabolism, including non-canonical activation of GCLC elevated

175   γ-glutamyl peptides and, GSSG depletion (Fig. 1l).

176   **Cysteine elimination drives adipose tissue browning.**

177   The decrease in fat mass during cysteine deficiency is driven by loss of all major fat depots

178   including subcutaneous fat (SFAT), visceral epididymal/ovarian adipose fat (VFAT), and brown

179   adipose tissue (BAT) (Extended data Fig. 2a). Histological analyses revealed that this reduction in

180   adipose tissue size is associated with transformation of white adipose depots into a BAT-like

181   appearance, with the formation of multilocular adipocytes, enlarged nuclei, and high UCP1

182   expression, a phenomenon known as 'browning' that increases thermogenesis[3,4] (Fig. 2a, b

183   Extended data Fig. 2b). Interestingly, the SFAT browning in cysteine-deficient mice was reduced

184   upon cysteine-restoration in diet (Fig. 2b). Similar response was observed in visceral fat (VFAT)

185   (Extended data 2b). Consistent with the browning of SFAT, the cysteine-deficient animals show

186   significantly increased expression of UCP1 (Fig 2c) and thermogenic marker genes (Fig. 2d). The

187   UCP1 and ATGL induction upon cysteine-deficiency in adipose tissue was reversed by cysteine-

188   repletion (Fig. 2c). Consistent with 30% weight-loss at day 5, the glycerol concentrations were

189   depleted in the sera of cysteine-deficient mice and were restored by cysteine-repletion induced

190   weight regain (Extended data Fig. 2c). The differentiation of Cth-deficient preadipocytes to mature

191   adipocytes and subsequent exposure to cysteine-free media did not affect thermogenic genes or

192   UCP1, suggesting that a non-cell autonomous mechanism may control adipocyte browning

193   (Extended data Fig. 2d).

194   We next investigate whether energy absorption, energy-intake or energy expenditure

195   contributes to the cysteine-depletion induced weight-loss. Analysis of energy absorption by fecal

196   bomb calorimetry revealed no significant difference in control and cysteine-deficient mice (Fig.

197   2e). Moreover, although the cumulative food intake over 5 days of weight loss was not statistically

198   different, the cumulative food intake in the first 2 days (Extended data Fig. 2d) after switching to

199   CysF diet was lower (p < 0.05) which may contribute to early weight loss. Calculation of the

200   analysis of covariance (ANCOVA) or representation of the data as regression between energy

201   expenditure and body mass[5,7], demonstrated that EE is increased in cysteine deficient animals

202   during the dark cycle (Fig. 2g) and not in the light cycle (Extended data Fig. 2f, g). In addition,

203   there was no difference in locomotor activity between control or cysteine-deficient mice (Extended

204   data Fig. 2h), suggesting cysteine depletion increases EE. Moreover, the increase in EE was

205   supported by increased fat utilization, as the respiratory exchange ratio (RER) in cysteine-deficient

206   animals was significantly reduced (Extended data Fig. 2i, j).

207   We next determined the specificity of cysteine on mechanisms that may contribute to rapid

208   weight loss. Interestingly, weight-regain post cysteine repletion significantly reversed adipose-

209   browning (Fig 2b, Extended data Fig. 2b) and normalized the glycerol, ATGL and UCP1 levels in

210   adipose tissue. (Fig. 2c). Furthermore, cysteine replacement also reversed the cysteine-deficiency-

211   induced reduction in RER, suggesting the restoration of organismal metabolism to carbohydrate

212   utilization instead of fatty acid oxidation (Fig. 2h, i). Surprisingly, cysteine repletion significantly

213   increased food intake for the first two days, suggesting that animals sense cysteine in diet and

214   compensate via hyperphagia to restore bodyweight setpoint (Fig. 2j). The EE upon cysteine-

215   replacement was not significantly different during weight rebound (Fig. 2k). These data suggest

216   that cysteine replacement can rapidly reverse weight loss by mechanisms that involve reduced

217   adipose browning, decreased fat utilization as well as increased energy intake.

218   We conducted the RNA-sequencing of the major adipose depots to investigate the

219   mechanisms that control adipose tissue browning and associated remodeling. As displayed by the

220   heatmap, cysteine deficiency profoundly alters the transcriptome of adipose tissue (Extended data

221   Fig. 2k). Gene set enrichment analysis comparing $Cth^{-/-}$ CTRL vs $Cth^{-/-}$ CysF identified that the

222   top downregulated pathways are involved in the extracellular matrix and collagen deposition,

223   highlighting the broad remodeling of the adipose tissue (Extended data Fig. 2l). In addition,

224   multiple metabolic pathways appear to be regulated by cysteine deficiency within the SFAT with

225   'respiratory electron transport chain and heat production' as the top pathway induced during

226   cysteine deficiency (Extended data Fig. 2l). Indeed, numerous genes identified by the

227   'thermogenesis' GO-term pathway such as *Ucp1, Cidea, Cox7a1, Cox8b, Dio2, Eva1, Pgc1,*

228   *Elovl3,* and *Slc27a2,* are differentially expressed comparing $Cth^{+/+}$ CysF and $Cth^{-/-}$ CysF in the

229   SFAT (Extended data Fig. 2m). These results demonstrate that cysteine depletion activates the

230   thermogenic transcriptional program.

231   To investigate the cellular basis of adipose tissue remodeling during cysteine deficiency,

232   we isolated stromal vascular fraction (SVF) by enzymatic digestion and conducted single-cell

233   RNA sequencing of SFAT. We isolated SVF cells from $Cth^{+/+}$ and $Cth^{-/-}$ fed CTRL or CysF diet

10

234   with each sample pooled from 4 animals (Extended data Fig. 3a). A total of 4,666 cells in $Cth^{+/+}$

235   CTRL; 5,658 cells in $Cth^{+/+}$ CysF; 4,756 cells in $Cth^{-/-}$ CTRL; and 3,786 cells in $Cth^{-/-}$ CysF were

236   analyzed for scRNA-seq (Extended data Fig. 3b). Consistent with prior results[30,31], the unbiased

237   clustering revealed 15 distinct cell populations including αβ T cells, γδ T cells, ILC2s, and NK T

238   cells, B cells, reticulocytes, mesothelial-like cells, Schwann cells, and several myeloid clusters

239   (Extended data Fig. 3b-d). Comparison of $Cth^{-/-}$ CysF with other groups revealed dramatic changes

240   in cellular composition (Fig. 2l). Particularly, loss of clusters 0, 1, and 2 were apparent upon

241   cysteine deficiency (Fig. 2l). Furthermore, these clusters contained the highest numbers of

242   differentially expressed genes induced by β3-adrenergic receptor agonist CL-316243[32] (Extended

243   data Fig. 3e), highlighting them as important cell populations in regulating the effects of cysteine

244   deficiency. By expression of $Pdgfra$, we identified these clusters as adipocyte progenitors (Fig.

245   2h). We conducted a pseudo-time analysis to place these clusters on a trajectory and illuminate

246   their cell lineage. Trajectory analysis based on pseudo-time suggested that cluster 2 may

247   differentiate into two separate preadipocyte clusters, clusters 0 and 1 (Fig. 2m). $Cth^{-/-}$ CysF animals

248   proportionally lost Clusters 0 and 1, while relatively maintaining cluster 2 compared to the other

249   groups (Fig. 2m), suggesting that more differentiated preadipocytes are mobilized during cysteine

250   deficiency. Indeed, cluster 2 expressed $Dpp4$, an early progenitor marker that has been shown to

251   give rise to different committed preadipoctyes[33] (Extended data Fig. 3f). Cluster 0 was enriched

252   for both $Icam1$ and $F3$, which are expressed by committed adipogenic, and antiadipogenic

253   preadipocytes, respectively [30,33] (Extended data Fig. 3g, h). $Cd9$, a fibrogenic marker in

254   preadipocytes [32,34], along with the collagen gene, $Col5a3,$ were broadly expressed across clusters

255   0 and 1, and was specifically lost by day 4 of inducing cysteine deficiency (Extended data Fig.

256   3g). The loss of these preadipocyte clusters were orthogonally validated by FACS (Extended data

257   Fig. 3h). We next sought to identify beige/brown adipocyte precursors in our scRNA-seq dataset

258   to understand whether there was an increased commitment towards brown adipocytes. Clearly,

259   *Tagln,* or Sm22, which has been previously described in beige adipocytes[35,36], is specifically

260   expressed by a subset of cells in cluster 1 (Extended data Fig. 3g). Interestingly, these *Tagln*-

261   expressing cells are lost with cysteine deficiency (Fig. 2i). Given the strong browning phenotype

262   observed on day 6, it is possible that these cells become mobilized and differentiate early on during

263   cysteine deficiency, leading to the absence of these cells as mature adipocytes are not captured

264   within the SVF. Indeed, when we performed pathways analysis on cluster1, comparing gene

265   expression of $Cth^{-/-}$ CysF with $Cth^{-/-}$ CTRL, we found that one of the top upregulated pathways

266   was 'adipogenesis' (Extended data Fig. 3i). Furthermore, examination of the expression of stem

267   associated markers and mature adipocyte markers in the adipocyte progenitor clusters revealed a

268   clear downregulation of stem markers and an increase in mature adipocyte markers, suggesting

269   that cysteine deficiency was driving the maturation of progenitor cells (Fig. 2m and Extended data

270   Fig. 3j). However, given the robust transformation of the adipose tissue during cysteine deficiency

271   towards browning, it is unlikely that mobilization of brown precursors alone is mediating this

272   response. Prior studies have found that in certain models, beige adipocytes can originate from pre-

273   existing white adipocytes, in addition to de-novo adipogenesis[37]. The potential role of cysteine in

274   the trans-differentiation of mature white adipocytes into brown-like adipocytes needs to be further

275   examined using future lineage-tracking studies.

276   **Cysteine depletion-induced FGF21 is partially required for weight loss.**

277   To determine the mechanism of adipose thermogenesis caused by cysteine starvation, we next

278   investigated the processes upstream of increased fatty acid oxidation. We measured the lipolysis

279   regulators pHSL and ATGL and found that cysteine deficiency increases ATGL expression

280 without consistently affecting pHSL levels (Fig. 3a, Extended data Fig. 4a). ATGL preferentially

281 catalyzes the first step of triglyceride hydrolysis whereas HSL has a much broader range of

282 substrates with a preference for diacylglycerols and cholesteryl esters[38]. Given a dramatic

283 browning response in WAT post-cysteine deficiency, the increased ATGL is consistent with prior

284 work that shows BAT relies heavily on the action of ATGL to mobilize lipid substrates for

285 thermogenesis[39]. This is further supported by a decrease in most lipid species, particularly

286 triglycerides and diacylglycerol in the BAT of cysteine deficient mice (Fig. 3b, Extended data Fig.

287 4b, c). Considering dramatic adipose tissue browning and elevated UCP1 expression upon cysteine

288 starvation, we next sought to investigate whether this is a homeostatic response to defend core-

289 body temperature (CBT) or if temperature set-point is perturbed to causes hyperthermia. We

290 measured core body temperature utilizing loggers surgically implanted into the peritoneal cavity

291 in $Cth^{-/-}$ mice on CTRL or CysF diet over 6 days period when animals lose weight. Surprisingly,

292 despite conversion of WAT into brown-like thermogenic fat, the core body temperature was not

293 different between control and cysteine deficient mice (Extended data Fig. 4d, e). These data

294 suggest that either cysteine- may signal the host to defend CBT within tight normal physiological

295 range or any metabolic heat that is generated is dissipated due to the animal housing in the

296 subthermoneutral temperature. To further confirm adipose thermogenesis *in vivo*, we utilized a

297 highly sensitive and specific magnetic resonance spectroscopic imaging (MRSI) method called

298 Biosensor Imaging of Redundant Deviation in Shifts (BIRDS)[40] to determine the temperature of

299 BAT in $Cth^{+/+}$ and $Cth^{-/-}$ animals after 6 days of CysF diet. This method relies on measuring the

300 chemical shift of the four non-exchangeable methyl groups from an exogenous contrast agent,

301 TmDOTMA, which has a high-temperature sensitivity (0.7 ppm/°C). The TmDOTMA- methyl

302 resonance has ultra-fast relaxation times (<5ms), allowing high signal-to-noise ratio by rapid

13

303   repetition for superior signal averaging[40]. The temperature was calculated from the chemical shift

304   of the TmDOTMA⁻ methyl resonance according to (eq. 1 methods). Compared to cysteine-replete

305   animals, the *in vivo* local temperature in BAT of cysteine-deficient mice was significantly greater

306   than surrounding tissue (Fig. 3c, d), suggesting increased thermogenesis.

307   Changes in nutritional stress induced by caloric restriction, methionine restriction, or low

308   protein diets upregulate the expression of FGF21, which, when overexpressed, increases lifespan

309   and also upregulates EE[41,42]. The induction of cysteine deficiency in *Cth* deficient mice caused a

310   dramatic increase in the FGF21 concentration in blood (Fig. 3e) and *Fgf21* expression in the liver

311   (Extended data Fig. 4f), which was reversed by cysteine-repletion induced weight regain (Fig 3e).

312   Similar to FGF21, the hormone GDF15, can also be induced by cellular or nutritional stress-

313   mediated signaling[43]. Cysteine depletion at day 4 post-weight loss significantly increased GDF15,

314   which was not restored after cysteine-repletion-induced weight regain (Fig 3f). Future studies are

315   required to determine if GDF15 is dispensable for cysteine-depletion-induced weight loss. Given

316   the cysteine-repleted diet switch increases food intake, the higher GDF15 levels during weight-

317   rebound are likely insufficient to cause food aversion.   Recent studies suggest elevated

318   endoplasmic-reticulum (ER) stress in *Bhmt⁻ᐟ⁻* mice with reduced methionine cycle, is associated

319   with increased FGF21 and adipose browning[44]. Notably, cysteine deficiency led to induction of

320   ER stress proteins CHOP, Calnexin, IRE1α and BIP (Fig. 3g). However, deletion of CHOP in

321   cysteine-starved mice did not rescue weight-loss (Fig. 3h) or affected the FGF21 and GDF15

322   serum levels (Extended data Fig. 4g,h) suggesting that CHOP dependent ER-stress response does

323   not drive cysteine's neuroendocrine or metabolic effect. Given cysteine specifically regulated

324   FGF21 during weight loss and regain (Fig 3e), we generated *Fgf21⁻ᐟ⁻ Cth⁻ᐟ⁻* DKO mice. In the

325   absence of FGF21, cysteine deficiency-induced weight-loss and reduction in adiposity in *Cth⁻ᐟ⁻*

326   mice were blunted, but the weight-loss trajectory continued and was not rescued (Fig. 3i, Extended

327   data Fig. 4i). The $Fgf21^{-/-} Cth^{-/-}$ DKO mice had lower EE compared to $Cth^{-/-}$ mice on CysF diet

328   (Fig. 3j). However, RER was not different, indicating that $Fgf21^{-/-} Cth^{-/-}$ mice still significantly

329   utilized fat as an energy substrate (Extended data Fig. 4j). This was supported by maintenance of

330   lipolysis signaling observed by levels of pHSL and ATGL in $Cth^{-/-}$ mice, but reduced UCP1 protein

331   and mRNA expression in WAT of $Fgf21^{-/-} Cth^{-/-}$ (Fig. 3k, Extended data Fig. 4k). Surprisingly,

332   the WAT of $Fgf21^{-/-} Cth^{-/-}$ DKO mice maintained classical multilocular browning characteristics

333   (Fig. 3l) suggesting that FGF21 is not required for adipose browning. These results suggest that

334   FGF21 is partially required for weight loss but does not mediate lipid mobilization or adipose

335   browning caused by cysteine deficiency.

336   Cysteine-starvation-induced weight-loss is maintained at thermoneutrality.

337   Cysteine elimination revealed a metabolic crisis that may signal the host to activate

338   thermogenic mechanisms. However, across animal vivaria, including ours, mice are housed at sub-

339   thermoneutral 20°C temperatures and are constantly under thermogenic stress due to slight cold

340   challenge[4]. To further confirm that mice were indeed inducing thermogenesis to defend core body

341   temperature, we housed cysteine deficient animals at 30°C thermoneutrality. The cysteine

342   deficiency in $Cth^{-/-}$ mice housed at 30°C also led to similar weight loss as 20°C with significant

343   browning of adipose tissue (Fig. 3m, n, Extended data Fig. 4l). The degree of browning and gene

344   expression of $Ucp1$ and $Elovl3$ in CysF Cth deficient mice at thermoneutrality was relatively lower

345   than inductions observed at 20°C (Fig. 3o). Furthermore, expression of genes involved with lipid

346   regulation and browning such as $Prdm16, Ppargc1a, Ppara, Pparg,$ and $Cpt1$ (Fig. 3p) were

347   significantly increased in SFAT, suggesting that even at thermoneutral temperatures, $Cth^{-/-}$ CysF

348   fed mice activate fat metabolism and, have increased thermogenesis caused by cysteine deficiency.

349 In addition, compared to controls, the cysteine deficient mice at thermoneutrality retained higher

350 UCP1 expression in BAT (Extended data Fig. 4m). Together, cysteine-depletion induced weight

351 loss and adipose browning are maintained at thermoneutrality.

Systemic depletion of cysteine drives browning in a UCP1-independent manner.

353 The liver is believed to be the primary organ for the maintenance of organismal cysteine

354 homeostasis[6,16]. Immunoblot analyses revealed the highest CTH expression in the liver followed

355 by the kidney, thymus, and adipose tissue (Extended data Fig. 5a). Given CR in humans lowers

356 cysteine in adipose tissue; we next generated adipocyte as well as hepatocyte-specific Cth deficient

357 mice to determine cell type-specific mechanism of cysteine in weight-loss (Fig. 4 a-f). As

358 expected, deletion of *Cth* in the liver did not affect the expression in the kidney, and adipose-

359 specific ablation of *Cth* maintained the expression in the liver (Extended data Fig. 5b). Neither

360 liver nor adipose-specific deletion of *Cth* caused a reduction in serum cysteine levels (Fig. 4c, d

361 and Extended data Fig. 5c,d) or fat-mass loss when cysteine was restricted in the diet (Fig. 4e, f).

362 The further LC/MS analyses of sera of hepatocyte-specific Cth deficient mice maintained on CysF

363 diet had no change in cystathionine, γ-glutamyl-dipeptides, cysteine or cystine (Fig 4 g, Extended

364 data Fig 5e). Consistent with low CTH activity, livers of the CysF-fed mice (AlbCre:*Cth*[f/f], CysF)

365 had lower levels of cysteine, cystathionine, s-adenosyl homocysteine, 2AB and ophthalmate

366 (Extended data Fig. 5f, g). Furthermore, cystathionine and cysteine/cystine in subcutaneous

367 adipose tissue of liver-specific Cth deficient mice were unchanged (Extended data Fig 5h, i)

368 suggesting specificity of TSP response in liver. Consistent with these data, no change in serum

369 cysteine/cystine were detected in adipose tissue specific Cth^{-/-} mice maintained on cysteine free

370 diet (Fig. 4h, Extended data Fig. 5j). The TSP metabolites can potentially be generated by the gut

371 microbiota[22]. The *Cth*^{-/-} animals co-housed together with *Cth*^{+/+} mice still maintained weight loss

372 when fed a CysF diet, suggesting that microbiota derived metabolites do not account for the

373 weight-loss (Extended data Fig. 5k). These results demonstrates that *Cth* across multiple tissues

374 may defend systemic cysteine concentration to prevent uncontrolled thermogenesis and death

375 when cysteine content is low in diet.

376 Given that UCP1 is a canonical regulator of non-shivering adipose thermogenesis[44,45] and

377 since cysteine-elimination induced UCP1 expression in WAT, we next deleted UCP1 in cysteine

378 deficient mice to determine its role in adipose browning. Interestingly, we found that $Cth^{-/-}Ucp1^{-/-}$

379 double knockout (DKO) mice had equivalent food intake (Extended data Fig. 5l) and lost weight

380 at a similar rate to its $Cth^{-/-}$ littermates on a CysF diet and displayed similar browning-like features

381 with multilocular adipocytes (Fig. 4i, j). The ablation of UCP1 in cysteine-deficient mice lowered

382 EE but did not affect the CBT (Fig. 4k, i). The lack of UCP1 in *Cth* deficient mice undergoing

383 cysteine starvation displayed elevated ATGL and tyrosine hydroxylase (TH) expression,

384 suggesting increased lipolytic signaling (Fig. 4m, n). Despite lack of UCP1, gene expression

385 indicative of the thermogenic program, such as *Ppargc1, Cidea, Cpt1* are significantly increased

386 in $Cth^{-/-} Ucp1^{-/-}$ DKO mice compared to $Cth^{-/-}$ in the BAT after 6 days of CysF diet (Fig. 4o).

387 Furthermore, gene expression of other mediators of the thermogenic genes such as *Acadm,*

388 *Cox7a1, Elovl3*, and *Slc27a2* are also significantly increased in $Cth^{-/-}Ucp1^{-/-}$ DKO mice compared

389 to $Cth^{-/-}$ animals fed cysteine-restricted diet (Fig. 4o). The UCP1-independent thermogenesis has

390 been reported[47]. The creatine futile cycling is proposed to regulate UCP1-independent

391 thermogenesis[48]. Compared to control animals, the creatine cycle genes *Ckb* and *Alpl* were not

392 significantly different in SFAT of cysteine-deficient animals (Extended data Fig. 5m). The creatine

393 synthesis genes, *Gatm* and *Gamt* were significantly reduced with cysteine deficiency in the SFAT

394 (Extended data Fig. 5m). The expression of one of the creatine kinases that utilize ATP, *Ckmt2*,

17

395 and the transporter for creatine, *Slc6a8* were also not differentially regulated in SFAT (Extended

396 data Fig. 5m). Interestingly, *Ckmt1* and *Ckmt2* expression was increased in BAT of *Cth$^{-/-}$Ucp1$^{-/-}$*

397 animals compared to cysteine-deficient animals (Fig. 4p). In addition, alternative UCP1-

398 independent thermogenic regulatory genes *Atp2a2* and *Ryr2* that control calcium cycling[49] were

399 not impacted by cysteine deficiency (Extended data Fig. 5n). Similarly, *Sarcolipin* and *Atp2a2* that

400 can increase muscle driven thermogenesis[50] were also not affected in skeletal muscle of *Cth*

401 deficient mice lacking cysteine (Extended data Fig. 5o). Futile lipid cycle is also implicated in

402 UCP1 independent thermogenesis[51]. Interestingly, *Cth$^{-/-}$* mice on CysF diet have significantly

403 elevated expression of *Dgat1*, *Pnpla2* and *Gk* with no change in *Lipe* in SFAT (Extended data Fig.

404 5p). The expression of these genes is also induced in absence of UCP1 in SFAT (Fig. 4q).

405 However, absence of association between changes in gene expression of major UCP1 independent

406 regulators does not rule out causal role of some of these mechanisms in cysteine-elimination driven

407 adipose browning. These results suggest that systemic cysteine deficiency-induced thermogenesis

408 depends on a non-canonical UCP1-independent thermogenic mechanism.

409

410 **Cysteine depletion-induced adipose browning and weight loss requires catecholamine**

411 **signaling.**

412 Since cysteine-elimination-induced adipocyte browning is non-cell autonomous (Extended

413 data Fig. 2d), we investigated the mechanism of adipose browning.

414 Upstream of lipolysis, non-shivering thermogenesis is mainly activated by the sympathetic

415 nervous system (SNS) derived adipose noradrenaline[52]. Mass-spectrometric analyses of

416 subcutaneous adipose tissue (Fig. 5a), including imaging mass spectrometry of BAT (Extended

417 data Fig. 6a) revealed that cysteine-starvation induced browning is associated with increased

18

418   noradrenaline (NA) concentrations. This was coupled with a significant reduction in NA-

419   degrading enzyme monoamine oxidase-a (*Maoa*), without affecting catechol-o-methyl transferase

420   (*Comt*), suggesting increased adipose NA bioavailability (Extended data Fig. 6b,c). Finally, to test

421   whether SNS derived NA is required for adipose browning, the inhibition of β3-adrenergic

422   receptors (ADRB3) by L748337 in *Cth* deficient mice lacking cysteine-protected animals against

423   weight loss (Fig. 5b), blunted adipose browning (Fig. 5c) and lowered browning marker *Ucp1*

424   (Fig. 5d). This was consistent with our unbiased RNA sequencing analyses that showed that

425   cysteine-regulated adipose clusters contained the highest numbers of differentially expressed

426   genes induced by β3-adrenergic receptor agonist (Extended data Fig. 3e). Together our findings

427   suggest that cysteine-depletion drives increased sympathetic activity leading to augmented

428   ADRB3-mediated NA signaling that controls adipose browning to weight loss.

429

430   **Cysteine deficiency reverses high-fat diet-induced obesity in mice.**

431   We next tested whether cysteine deficiency could be utilized to induce an adaptive thermogenic

432   mechanism for fat mass reduction in the high-fat diet (HFD) induced obesity model. The $Cth^{-/-}$

433   mice that had been fed HFD for 12 weeks were switched to an isocaloric HFD containing (HFD-

434   CTRL) or lacking cystine (HFD-CysF). The $Cth^{-/-}$ mice fed HFD-CysF diet were able to lose

435   approximately 30% body weight within 1 week despite maintaining a high calorie intake (Fig. 5e).

436   This weight loss was associated with major reductions in fat mass (Extended Fig. 6d). With weight

437   loss, cysteine deficient mice had improved metabolic homeostasis, (Fig. 5f and Extended data Fig.

438   6e,f), increased EE (Fig. 5g,h). Notably, immuno-histological analysis of the white adipose depots

439   demonstrated that cysteine deficiency induced browning even while on HFD with increased

440   expression of UCP1 in SFAT and VFAT (Fig. 5i). Furthermore, cysteine-deficiency in obese mice

19

441   reduced RER suggesting higher fat-utilization (Fig. 5j). Additionally, consistent with improvement

442   of metabolic function in obesity, the gene expression of inflammasome components *Il1b, Il18,*

443   *Nlrp3, Casp1* and pro-inflammatory cytokines *Il6* and *Tnf* were reduced in F4/80^{+}CD11b^{+} adipose

444   tissue macrophages in visceral adipose tissue (Fig. 5k) These results demonstrate that induction of

445   cysteine deficiency can cause weight-loss in mouse model of diet-induced obesity, opening new

446   avenues for future drug development for excess weight-loss

447

448   **Discussion**

449   Adipose tissue regulates metabolism by orchestrating inter-organ communication required for

450   healthy longevity[53]. Analyses of adipose tissue of humans that underwent moderate CR in free-

451   living conditions have highlighted genes and pathways that link energy metabolism and

452   inflammation to influence healthspan[5, 7]. In rodents, restriction of calories up to 40% reduces core-

453   body temperature (CBT) and induces browning of the adipose tissue of mice reared in sub-

454   thermoneutral temperature[1]. The CR in humans upregulated the fatty acid oxidation and futile lipid

455   cycling induced-thermogenic pathways but UCP1 was undetectable in adipose tissue of

456   CALERIE-II participants[5]. Similarly, weight loss in obese humans is not associated with classical

457   UCP1 adipose tissue browning[54]. This suggests that alternate UCP1-independent mechanisms

458   maybeat play in human and rodent adipose tissue browning and thermogenesis in response to CR,

459   may be due to extreme CR (>40%) or another phenomenon, including reduction of specific amino

460   acids or macronutrients. In this regard, reduction of core-body temperature[55] and increased FGF21

461   is a common link between CR and MR-induced adipose browning and increased longevity[1,2,42].

462   Our studies demonstrated that reduction of cysteine and subsequent rewiring of downstream

463   cysteine metabolism is linked to adipose browning and weight loss.

20

464   Expression and activity of TSP genes CBS and CTH increase when cysteine is low[6]. Indeed, during CR, the TSP is induced to defend against the depletion of cysteine levels. MR regimens that improve lifespan are also restricted or deficient in cysteine[15], and it is unclear whether methionine or cysteine restriction drives pro-longevity effects. Thus, to understand the metabolic requirement of dietary non-essential amino acid such as cysteine, a genetic mouse model is required that lacks *Cth* in conjunction with restriction of cysteine. Surprisingly, previously reported *Cth* mutant mice originally generated on a 129SvEv mouse strain maintained on cysteine-replete normal chow diet were reported to display hypertension and motor-dysfunction characteristic of neurodegenerative changes in corpus striatum[56,57]. Through conditional deletion of *Cth* (on pure C57/B6 background) in adipose tissue and liver, and rescue of weight-loss by cysteine repletion, our data establishes that systemic cysteine depletion drives adipose tissue thermogenesis without causing behavioral defects or pathological lesions.

476   While it is still unclear why cysteine deficiency triggers the activation of adipose browning, the mechanism of thermogenesis depends on sympathetic β3-adrenergic signaling and partially requires FGF21 and can be successfully maintained even in the absence of UCP1 and at thermoneutrality. The cysteine-starvation elevated fatty acid lipolysis-esterification cycle genes, while the genes regulating calcium and creatine cycle were not affected. Future studies of specific ablation of UCP1-independent thermogenic genes in $Cth^{-/-}$ mice on cysteine-restriction are required to determine the causal pathway. The model of cysteine loss that produces a strong browning response may thus allow the discovery of an alternate UCP1-independent mechanism of adipose tissue thermogenesis.

485   In healthy humans undergoing CR, consistent with reduced cysteine, glutathione, a major redox regulator, was reduced in adipose tissue. The *Cth* deficient mice on a cysteine-free diet show

487   a decrease in oxidized GSH with a compensatory increase in *Gclc*, *Gss*, and accumulation of γ-

488   glutamyl-peptides. Despite increased oxidative stress, the adipose tissue histology, RNA

489   sequencing, and lipidomic analysis of BAT did not reveal overt ferroptosis in cysteine-depletion

490   induced weight loss. Future studies may reveal cysteine-dependent alternative protective

491   mechanisms that control redox balance and ferroptosis while sustaining UCP1-independent

492   thermogenesis.

493   Taken together, this study expands our understanding of pathways activated by pro-

494   longevity dietary interventions that confer metabolic adaptation required to maintain tissue

495   homeostasis. Thus, the manipulation of TSP activity to drive adipose tissue browning also has

496   implications for developing interventions that control adiposity and promote longevity. In humans,

497   restriction of methionine and cysteine increased FGF21 and caused a reduction in body weight

498   with improvement of metabolic parameters[58]. Similar to our findings, the metabolic benefits of

499   methionine+cysteine dietary restriction in humans were greater than methionine- restriction

500   alone[58]. Here, based on human dietary restriction studies, and mouse models of cysteine-

501   deficiency, we demonstrate that cysteine is essential for organismal metabolism as its absence

502   triggers adipose browning with progressive weight loss.

503

504

505

506

507

508

509

Acknowledgments

Citations

1. Fabbiano S, Suárez-Zamorano N, Rigo D, Veyrat-Durebex C, Stevanovic Dokic A, Colin DJ, Trajkovski M. Caloric Restriction Leads to Browning of White Adipose Tissue through Type 2 Immune Signaling. Cell Metab. 2016 Sep 13;24(3):434-446.

2. Wanders D, Forney LA, Stone KP, Burk DH, Pierse A, Gettys TW. FGF21 Mediates the Thermogenic and Insulin-Sensitizing Effects of Dietary Methionine Restriction but Not Its Effects on Hepatic Lipid Metabolism. Diabetes. 2017 Apr;66(4):858-867.

3. Chouchani ET, Kazak L, Spiegelman BM. New Advances in adaptive Thermogenesis: UCP1 and Beyond. Cell Metab. 2019 Jan 8;29(1):27-37.

4. Cannon B, Nedergaard J. Brown adipose tissue: function and physiological significance. Physiol Rev. 2004 Jan;84(1):277-359.

5. Spadaro O, Youm Y, Shchukina I, Ryu S, Sidorov S, Ravussin A, Nguyen K, Aladyeva E, Predeus AN, Smith SR, Ravussin E, Galban C, Artyomov MN, Dixit VD. Caloric restriction in humans reveals immunometabolic regulators of health span. Science. 2022 Feb 11;375(6581):671-677.

6. Stipanuk MH. Metabolism of sulfur-containing amino acids. Annu. Rev. Nutr. 1986, 6: 179-209.

7. Ryu S, Sidorov S, Ravussin E, Artyomov M, Iwasaki A, Wang A, Dixit VD. The matricellular protein SPARC induces inflammatory interferon-response in macrophages during aging. Immunity. 2022 Sep 13;55(9):1609-1626.

8. Redman LM, Smith SR, Burton JH, Martin CK, Il'yasova D, Ravussin E. Metabolic Slowing and Reduced Oxidative Damage with Sustained Caloric Restriction Support the Rate of Living and Oxidative Damage Theories of Aging. Cell Metab. 2018 Apr 3;27(4):805-815

9. Green CL, Lamming DW, Fontana L. Molecular mechanisms of dietary restriction promoting health and longevity. Nat Rev Mol Cell Biol. 2022 Jan;23(1):56-73.

10. Grandison RC, Piper MD, Partridge L. Amino-acid imbalance explains extension of lifespan by dietary restriction in Drosophila. Nature. 2009 Dec 24;462(7276):1061-4

11. Orentreich N, Matias JR, DeFelice A, Zimmerman JA (1993) Low methionine ingestion by rats extends life span. J Nutr 123:269–27.

12. Xu, Q., Li, Y., Gao, X. *et al.* HNF4α regulates sulfur amino acid metabolism and confers sensitivity to methionine restriction in liver cancer. Nat Commun. 2020 Aug 7;11(1):3978.

13. Plaisance EP, Henagan TM, Echlin H, Boudreau A, Hill KL, Lenard NR, Hasek BE, Orentreich N, Gettys TW. Role of beta-adrenergic receptors in the hyperphagic and hypermetabolic responses to dietary methionine restriction. Am J Physiol Regul Integr Comp Physiol. 2010 Sep;299(3):R740-50.

14. Johnson DC, Dean DR, Smith AD, Johnson MK. Structure, function, and formation of biological iron-sulfur clusters. Annu Rev Biochem. 2005;74:247-81.

15. Elshorbagy AK, Valdivia-Garcia M, Mattocks DA, Plummer JD, Smith AD, Drevon CA, Refsum H, Perrone CE. Cysteine supplementation reverses methionine restriction effects on rat adiposity: significance of stearoyl-coenzyme A desaturase. J Lipid Res. 2011 Jan;52(1):104-12.

16. Deplancke B, Gaskins HR. Redox control of the transsulfuration and glutathione biosynthesis pathways. Curr Opin Clin Nutr Metab Care. 2002 Jan;5(1):85-92.

17. Moosmann B, Schindeldecker M, Hajieva P. Cysteine, glutathione and a new genetic code: biochemical adaptations of the primordial cells that spread into open water and survived biospheric oxygenation. Biol Chem. 2020 Feb 25;401(2):213-231.

18. Jordan SF, Ioannou I, Rammu H, Halpern A, Bogart LK, Ahn M, Vasiliadou R, Christodoulou J, Maréchal A, Lane N. Spontaneous assembly of redox-active iron-sulfur clusters at low concentrations of cysteine. Nat Commun. 2021 Oct 11;12(1):5925.

19. Uthus EO, Brown-Borg HM. Methionine flux to transsulfuration is enhanced in the long living Ames dwarf mouse. Mech Ageing Dev. 2006 May;127(5):444-50.

20. Hine C, Harputlugil E, Zhang Y, Ruckenstuhl C, Lee BC, Brace L, Longchamp A, Treviño-Villarreal JH, Mejia P, Ozaki CK, Wang R, Gladyshev VN, Madeo F, Mair WB, Mitchell JR. Endogenous hydrogen sulfide production is essential for dietary restriction benefits. Cell. 2015 Jan 15;160(1-2):132-44.

21. Tyshkovskiy A, Bozaykut P, Borodinova AA, Gerashchenko MV, Ables GP, Garratt M, Khaitovich P, Clish CB, Miller RA, Gladyshev VN. Identification and Application of Gene Expression Signatures Associated with Lifespan Extension. Cell Metab. 2019 Sep 3;30(3):573-593.e8.

22. Shalayel I, Youssef-Saliba S, Vazart F, Ceccarelli C, Bridoux M, Vallée Y. Cysteine chemistry in connection with abiogenesis. European J. Org. Chem. 2020, 3019–3023 (2020).

23. Kang YP, Mockabee-Macias A, Jiang C, Falzone A, Prieto-Farigua N, Stone E, Harris IS, DeNicola GM. Non-canonical Glutamate-Cysteine Ligase Activity Protects against Ferroptosis. Cell Metab. 2021 Jan 5;33(1):174-189.e7.

24. Fujii J, Osaki T, Soma Y, Matsuda Y. Critical Roles of the Cysteine-Glutathione Axis in the Production of γ-Glutamyl Peptides in the Nervous System. Int J Mol Sci. 2023 Apr 28;24(9):8044.

25. LIEN OG Jr, GREENBERG DM. Identification of alpha-aminobutyric acid enzymatically formed from threonine. J Biol Chem. 1953 Jan;200(1):367-71.

26. Seelig GF, Simondsen RP, Meister A. Reversible dissociation of gamma-glutamylcysteine synthetase into two subunits. J Biol Chem. 1984 Aug 10;259(15):9345-7

27. Huang CS, Chang LS, Anderson ME, Meister A. Catalytic and regulatory properties of the heavy subunit of rat kidney gamma-glutamylcysteine synthetase. J Biol Chem. 1993 Sep 15;268(26):19675-80.

28. Rouault TA. Mammalian iron-sulphur proteins: novel insights into biogenesis and function. Nat Rev Mol Cell Biol. 2015 Jan;16(1):45-55.

29. Tajima K, Ikeda K, Chang HY, Chang CH, Yoneshiro T, Oguri Y, Jun H, Wu J, Ishihama Y, Kajimura S. Mitochondrial lipoylation integrates age-associated decline in brown fat thermogenesis. Nat Metab. 2019 Sep;1(9):886-898.

30. Emont MP, Jacobs C, Essene AL, Pant D, Tenen D, Colleluori G, Di Vincenzo A, Jørgensen AM, Dashti H, Stefek A, McGonagle E, Strobel S, Laber S, Agrawal S, Westcott GP, Kar A, Veregge ML, Gulko A, Srinivasan H, Kramer Z, De Filippis E, Merkel E, Ducie J, Boyd CG, Gourash W, Courcoulas A, Lin SJ, Lee BT, Morris D, Tobias A, Khera AV, Claussnitzer M, Pers TH, Giordano

24

A, Ashenberg O, Regev A, Tsai LT, Rosen ED. A single-cell atlas of human and mouse white adipose tissue. Nature. 2022 Mar;603(7903):926-933.

31. Goldberg EL, Shchukina I, Youm YH, Ryu S, Tsusaka T, Young KC, Camell CD, Dlugos T, Artyomov MN, Dixit VD. IL-33 causes thermogenic failure in aging by expanding dysfunctional adipose ILC2. Cell Metab. 2021 Nov 2;33(11):2277-2287.

32. Burl RB, Ramseyer VD, Rondini EA, Pique-Regi R, Lee YH, Granneman JG. Deconstructing adipogenesis induced by β3-adrenergic receptor activation with single-cell expression profiling. Cell Metab. 2018 Aug 7;28(2):300-309.e

33. Merrick D, Sakers A, Irgebay Z, Okada C, Calvert C, Morley MP, Percec I, Seale P Identification of a mesenchymal progenitor cell hierarchy in adipose tissue. Science. 2019 Apr 26;364(6438):eaav2501.

34. Marcelin G, Silveira ALM, Martins LB, Ferreira AV, Clément K. Deciphering the cellular interplays underlying obesity-induced adipose tissue fibrosis. J Clin Invest. 2019 Oct 1;129(10):4032-4040.

35. Berry DC, Jiang Y, Graff JM. Mouse strains to study cold-inducible beige progenitors and beige adipocyte formation and function. Nat Commun. 2016 Jan 5;7:10184.

36. Oguri Y, Shinoda K, Kim H, Alba DL, Bolus WR, Wang Q, Brown Z, Pradhan RN, Tajima K, Yoneshiro T, Ikeda K, Chen Y, Cheang RT, Tsujino K, Kim CR, Greiner VJ, Datta R, Yang CD, Atabai K, McManus MT, Koliwad SK, Spiegelman BM, Kajimura S. CD81 Controls Beige Fat Progenitor Cell Growth and Energy Balance via FAK Signaling. Cell. 2020 Aug 6;182(3):563-577.e20.

37. Lee YH, Petkova AP, Mottillo EP, Granneman JG. In vivo identification of bipotential adipocyte progenitors recruited by β3-adrenoceptor activation and high-fat feeding. Cell Metab. 2012 Apr 4;15(4):480-91.

38. Zimmermann R, Strauss JG, Haemmerle G, Schoiswohl G, Birner-Gruenberger R, Riederer M, Lass A, Neuberger G, Eisenhaber F, Hermetter A, Zechner R. Fat mobilization in adipose tissue is promoted by adipose triglyceride lipase. Science. 2004 Nov 19;306(5700):1383-6.

39. Morak M, Schmidinger H, Riesenhuber G, Rechberger GN, Kollroser M, Haemmerle G, Zechner R, Kronenberg F, Hermetter A. Adipose triglyceride lipase (ATGL) and hormone-sensitive lipase (HSL) deficiencies affect expression of lipolytic activities in mouse adipose tissues. Mol Cell Proteomics. 2012 Dec;11(12):1777-89.

40. Coman D, Trubel HK, Hyder F. Brain temperature by Biosensor Imaging of Redundant Deviation in Shifts (BIRDS): comparison between TmDOTP5- and TmDOTMA-. NMR Biomed. 2010 Apr;23(3):277-85.

41. Kliewer SA, Mangelsdorf DJ. A Dozen Years of Discovery: Insights into the Physiology and Pharmacology of FGF21. Cell Metab. 2019 Feb 5;29(2):246-253.

42. Hill CM, Albarado DC, Coco LG, Spann RA, Khan MS, Qualls-Creekmore E, Burk DH, Burke SJ, Collier JJ, Yu S, McDougal DH, Berthoud HR, Münzberg H, Bartke A, Morrison CD. FGF21 is required for protein restriction to extend lifespan and improve metabolic health in male mice. Nat Commun. 2022 Apr 7;13(1):1897

43. Patel S, Alvarez-Guaita A, Melvin A, Rimmington D, Dattilo A, Miedzybrodzka EL, Cimino I, Maurin AC, Roberts GP, Meek CL, Virtue S, Sparks LM, Parsons SA, Redman LM, Bray GA, Liou AP, Woods RM, Parry SA, Jeppesen PB, Kolnes AJ, Harding HP, Ron D, Vidal-Puig A, Reimann F, Gribble FM, Hulston CJ, Farooqi IS, Fafournoux P, Smith SR, Jensen J, Breen D, Wu Z, Zhang BB, Coll AP, Savage DB, O'Rahilly S. GDF15 Provides an Endocrine Signal of Nutritional Stress in Mice and Humans. Cell Metab. 2019 Mar 5;29(3):707-718.e8.

44. Warrier M, Paules EM, Silva-Gomez J, Friday WB, Bramlett F, Kim H, Zhang K, Trujillo-Gonzalez I. Homocysteine-induced endoplasmic reticulum stress activates FGF21 and is associated with browning and atrophy of white adipose tissue in Bhmt knockout mice. Heliyon. 2023 Jan 28;9(2):e13216.

45. Nicholls DG Mitochondrial proton leaks and uncoupling proteins. Biochim Biophys Acta Bioenerg. 2021 Jul 1;1862(7):148428.

46. Kozak LP, Harper ME. Mitochondrial uncoupling proteins in energy expenditure. Annu Rev Nutr. 2000;20:339-63.

47. Ukropec J, Anunciado RP, Ravussin Y, Hulver MW, Kozak LP. UCP1 independent thermogenesis in white adipose tissue of cold-acclimated Ucp1-/- mice. J Biol Chem. 2006 Oct 20;281(42):31894-908.

48. Kazak L, Chouchani ET, Jedrychowski MP, Erickson BK, Shinoda K, Cohen P, Vetrivelan R, Lu GZ, Laznik-Bogoslavski D, Hasenfuss SC, Kajimura S, Gygi SP, Spiegelman BM A creatine-driven substrate cycle enhances energy expenditure and thermogenesis in beige fat. Cell. 2015 Oct 22;163(3):643-55.

49. Ikeda K, Kang Q, Yoneshiro T, Camporez JP, Maki H, Homma M, Shinoda K, Chen Y, Lu X, Maretich P, Tajima K, Ajuwon KM, Soga T, Kajimura S. UCP1-independent signaling involving SERCA2b-mediated calcium cycling regulates beige fat thermogenesis and systemic glucose homeostasis. Nat Med. 2017 Dec;23(12):1454-1465.

50. Bal NC, Maurya SK, Sopariwala DH, Sahoo SK, Gupta SC, Shaikh SA, Pant M, Rowland LA, Bombardier E, Goonasekera SA, Tupling AR, Molkentin JD, Periasamy M. Sarcolipin is a newly identified regulator of muscle-based thermogenesis in mammals. Nat Med. 2012 Oct;18(10):1575-9.

51. Oeckl J, Janovska P, Adamcova K, Bardova K, Brunner S, Dieckmann S, Ecker J, Fromme T, Funda J, Gantert T, Giansanti P, Hidrobo MS, Kuda O, Kuster B, Li Y, Pohl R, Schmitt S, Schweizer S, Zischka H, Zouhar P, Kopecky J, Klingenspor M. Loss of UCP1 function augments recruitment of futile lipid cycling for thermogenesis in murine brown fat. Mol Metab. 2022 Jul;61:101499.

52. Bartness TJ, Bamshad M. Innervation of mammalian white adipose tissue: implications for the regulation of total body fat. Am J Physiol. 1998 Nov;275(5):R1399-411.

53. Lee AH, Dixit VD. Dietary Regulation of Immunity. Immunity. 2020 Sep 15;53(3):510-523.

54. Barquissau V, Léger B, Beuzelin D, Martins F, Amri EZ, Pisani DF, Saris WHM, Astrup A, Maoret JJ, Iacovoni J, Déjean S, Moro C, Viguerie N, Langin D. Caloric Restriction and Diet-Induced Weight Loss Do Not Induce Browning of Human Subcutaneous White Adipose Tissue in Women and Men with Obesity. Cell Rep. 2018 Jan 23;22(4):1079-1089.

55. Conti B, Sanchez-Alavez M, Winsky-Sommerer R, Morale MC, Lucero J, Brownell S, Fabre V, Huitron-Resendiz S, Henriksen S, Zorrilla EP, de Lecea L, Bartfai T. Transgenic mice with a reduced core body temperature have an increased life span. Science. 2006 Nov 3;314(5800):825-8.

56. Yang G, Wu L, Jiang B, Yang W, Qi J, Cao K, Meng Q, Mustafa AK, Mu W, Zhang S, Snyder SH, Wang R. H2S as a physiologic vasorelaxant: hypertension in mice with deletion of cystathionine gamma-lyase. Science. 2008 Oct 24;322(5901):587-90.

57. Paul BD, Sbodio JI, Xu R, Vandiver MS, Cha JY, Snowman AM, Snyder SH Cystathionine γ-lyase deficiency mediates neurodegeneration in Huntington's disease. Nature. 2014 May 1;509(7498):96-100.

58. Richie JP Jr, Sinha R, Dong Z, Nichenametla SN, Ables GP, Ciccarella A, Sinha I, Calcagnotto AM, Chinchilli VM, Reinhart L, Orentreich D. Dietary Methionine and Total Sulfur Amino Acid Restriction in Healthy Adults. J Nutr Health Aging. 2023;27(2):111-123.

59. Nakai K, Kadiiska MB, Jiang JJ, Stadler K, Mason RP. Free radical production requires both inducible nitric oxide synthase and xanthine oxidase in LPS-treated skin. Proc Natl Acad Sci U S A. 2006 Mar 21;103(12):4616-21.

699   **Materials and methods**

700

701   **Human Samples**

702   The participants in this study were part of the CALERIE Phase 2 (Rochon et al., 2011) study which

703   was a multi-center, parallel-group, randomized controlled trial by recruitment of non-obese healthy

704   individuals. 238 adults participated at 3 different locations: Pennington Biomedical Research

705   Center (Baton Rouge, LA), Washington University (St. Louis, MO) and Tufts University (Boston,

706   MA) (NCT00427193). Duke University, (Durham, NC) served as a coordinating center.

707   Participants were randomly assigned to of 25% caloric restriction or ad libitum caloric intake for

708   two years. CR group participants actually reached 14% of CR[5,8] (Ravussin et al. 2015). Men were

709   between 20 and 50 years old and women were between 20 and 47 years old. Their body mass index

710   (BMI) was between 22.0 and 27.9 kg/m^2 at the initial visit. Samples were collected at baseline, 1

711   year, and 2 years of intervention. Abdominal subcutaneous adipose tissue biopsy was performed

712   on a portion of CR group participants and used for RNA-sequencing and metabolomics in this

713   study. All studies were performed under protocol approved by the Pennington institutional review

714   board with informed consent from participants.

715   **Mice**

716   All mice were on the C57BL/6J (B6) genetic background. $Cth^{-/-}$ mice (C57BL/6NTac-

717   Cth[tm1a(EUCOMM)Hmgu/Ieg]) were purchased from the European Mouse Mutant Cell Repository.

718   Breeding these mice to Flipase transgenic mice from Jackson Laboratories generated $Cth^{fl/fl}$ mice

719   which were crossed to Adipoq-cre and Albumin-cre, purchased from Jackson Laboratories. $Ucp1^{-/-}$

720   and CHOP$^{-/-}$ mice were purchased from Jackson laboratories and crossed to $Cth^{-/-}$ mice. $Fgf21^{-/-}$

721   mice were kindly provided by Dr. Steven Kliewer (UT Southwestern) as described previously[41]

27

722   and crossed to *Cth*^{-/-} mice. All mice used in this study were housed in specific pathogen-free

723   facilities in ventilated cage racks that deliver HEPA-filtered air to each cage with free access to

724   sterile water through a Hydropac system at Yale School of Medicine. Mice were fed a standard

725   vivarium chow (Harlan 2018s) unless special diet was provided and housed under 12 h light/dark

726   cycles. All experiments and animal use were approved by the Institutional Animal Care and Use

727   Committee (IACUC) at Yale University.

728   **Diet studies**

729   For cysteine deficiency studies, mice were fed either a control diet, CysF diet, HFD-CTRL diet,

730   or HFD-CysF diet purchased from Dyets, for 6 days unless specified otherwise. For pair feeding

731   studies, mice were provided with either ad libitum or 2.22-2.27g of diet daily.

732   **Western blot analysis**

733   Cell lysates were prepared using RIPA buffer and optionally frozen and stored at -80°C. Samples

734   were left on ice, vortexing every ten min for 30 min. For tissue samples, snap frozen tissues were

735   ground by mortar and pestle in liquid nitrogen and resuspended in RIPA buffer with protease and

736   phosphatase inhibitors. Samples were centrifuged at 14,000g for 15min and the supernatant was

737   collected protein concentration was determined using the DC Protein Assay (Bio-Rad) and

738   transferred to a nitrocellulose membrane. The following antibodies (and source) were used to

739   measure protein expression: β-Actin (Cell Signaling), pHSL p660 (Cell Signaling), ATGL (Cell

740   Signaling), UCP1 (Abcam), CSE (Novus), Tubulin (Sigma), HSL (Cell Signaling), COMT

741   (Biorad), MAOA (Abcam), TH (Cell Signaling), IRE1a (Cell Signaling), Calnexin (Cell

742   Signaling), BiP (Cell Signaling), CHOP (Cell Signaling), HSP90 (Cell Signaling); followed by

743   incubation with appropriate HRP-conjugated secondary antibodies (Thermo Fisher Scientific).

744

Gene expression analysis

Cells or ground tissue (described above) were collected in STAT-60 (Tel-test). RNA from cells were extracted using Qiagen RNeasy micro kits following manufacturer's instructions. For tissue samples, RNA was extracted using Zymo mini kits following manufacturer's instructions. During RNA extraction, DNA was digested using RNase free DNase set (Qiagen). Synthesis of cDNA was performed using iScript cDNA synthesis kit (Bio-Rad) and real time quantitative PCR (Q-PCR) was conducted using Power SYBR Green detection reagent (Thermo Fischer Scientific) on a Light Cycler 480 II (Roche).

Glucose tolerance test

$Cth^{-/-}$ HFD-CTRL and HFD-CysF mice were fasted 14hr prior to glucose tolerance test. Glucose was given by i.p. injection based on body weight (0.4g/kg). $Cth^{-/-}$ CTRL and CysF mice were fasted for 4hr. Glucose was given by i.p based on lean mass determined by Echo-MRI (2g/kg of lean mass). Blood glucose levels were measured by handheld glucometer (Breeze, Bayer Health Care).

Flow Cytometry

Adipose tissue was digested at 37°C in HBSS (Life Technologies) + 0.1% collagenase I or II (Worthington Biochemicals). The stromal vascular fraction was collected by centrifugation, washed and filtered using 100um and 70um strainers. Cells were stained with LIVE/DEAD™ Fixable Aqua Dead Cell Stain Kit (Thermo Fisher Scientific) and then for surface markers including CD45, CD3, B220, CD11b, F4/80, Ly6G, Siglec F, CD163, CD24, F3, CD31, Pdgfra,

29

767   Dpp4, and CD9 and all antibodies were purchased from eBioscience or Biolegend. Cells were

768   fixed in 2% PFA. Samples were acquired on a custom LSR II and data was analyzed in FlowJo.

769

770   **Single-cell RNA sequencing**

771   For stromal vascular fraction, female $Cth^{+/+}$ and $Cth^{-/-}$ mice were fed CTRL of CysF diet for 4

772   days. SFAT was collected, with lymph nodes removed, pooled, and digested. Isolated cells were

773   subjected to droplet-based 3' end massively parallel single-cell RNA sequencing using Chromium

774   Single Cell 3' Reagent Kits as per manufacturer's instructions (10x Genomics). The libraries were

775   sequenced using a HiSeq3000 instrument (Illumina). Sample demultiplexing, barcode processing,

776   and single-cell 3' counting was performed using the Cell Ranger Single-Cell Software Suite (10x

777   Genomics). Cellranger count was used to align samples to the reference genome (mm10), quantify

778   reads, and filter reads with a quality score below 30. The Seurat package in R was used for

779   subsequent analysis[31]. Cells with mitochondrial content greater than 0.05% were removed and data

780   was normalized using a scaling factor of 10,000, and nUMI was regressed with a negative binomial

781   model. Principal component analysis was performed using the top 3000 most variable genes and

782   t-SNE analysis was performed with the top 20 PCAs. Clustering was performed using a resolution

783   of 0.4. The highly variable genes were selected using the FindVariableFeatures function with mean

784   greater than 0.0125 or less then 3 and dispersion greater than 0.5. These genes are used in

785   performing the linear dimensionality reduction. Principal component analysis was performed prior

786   to clustering and the first 20 PC's were used based on the ElbowPlot. Clustering was performed

787   using the FindClusters function which works on K-nearest neighbor (KNN) graph model with the

788   granularity ranging from 0.1-0.9 and selected 0.4 for the downstream clustering. For identifying

789   the biomarkers for each cluster, we have performed differential expression between each cluster

790   to all other clusters identifying positive markers for that cluster. To understand the trajectory of

791   the adipocyte progenitors, we used Monocle2 to analyze scRNA-seq data of Clusters 0, 1, and 2

792   (Trapnell 2014).

Whole tissue RNA sequencing and transcriptome analysis

794   Snap frozen tissues were ground by mortar and pestle in liquid nitrogen and resuspended in STAT-

795   60. RNA was extracted using Zymo mini kits. RNA was sequenced on a HiSeq2500. The quality

796   of raw reads was assessed with FastQC [FastQC]. Raw reads were mapped to the GENCODE vM9

797   mouse reference genome [GENCODE] using STAR aligner [STAR] with the following options: -

798   -outFilterMultimapNmax 15 --outFilterMismatchNmax 6 --outSAMstrandField All --

799   outSAMtype BAM SortedByCoordinate --quantMode TranscriptomeSAM. The quality control of

800   mapped reads was performed using in-house scripts that employ Picard tools [Picard][5]. The list of

801   rRNA genomic intervals that we used for this quality control was prepared on the basis of UCSC

802   mm10 rRNA annotation file [UCSC] and GENCODE primary assembly annotation for vM9

803   [GENCODE]. rRNA intervals from these two annotations were combined and merged to obtain

804   the final list of rRNA intervals. These intervals were used for the calculation of the percentage of

805   reads mapped to rRNA genomic loci. Strand specificity of the RNA-Seq experiment was

806   determined using an in-house script, on the basis of Picard [Picard] mapping statistics. Expression

807   quantification was performed using RSEM [RSEM]. For the assessment of expression of

808   mitochondrial genes, we used all genes annotated on the mitochondrial chromosome in the

809   GENCODE vM9 mouse reference genome [GENCODE]. PCA was performed in R. For the PCA,

810   donor effect was removed using the ComBat function from the sva R-package [sva]. Gene

811   differential expression was calculated using DESeq2 [DESeq2].]. Pathway analysis was done

812   using fgsea (fast GSEA) R-package [fgsea] with the minimum of 15 and maximum of 500 genes

813   in a pathway and with 1 million of permutations. For the pathway analysis, we used the Canonical

814   Pathways from the MSigDB C2 pathway set [MSigDB1, MSigDB2], v6.1. The elimination of

815   redundant significantly regulated pathways (adjusted p-value < 0.05) was done using an in-house

816   Python script in the following way. We considered all ordered pairs of pathways, where the first

817   pathway had normalized enrichment score equal to or greater than the second pathway. For each

818   ordered pair of pathways, we analyzed the leading gene sets of these pathways. The leading gene

819   sets were obtained using fgsea [fgsea]. If at least one of the leading gene sets in a pair of pathways

820   had more than 60% of genes in common with the other leading gene set, then we eliminated the

821   second pathway in the pair.

822   **Sample preparation for metabolome analysis**

823   Frozen tissues or serum samples, together with internal standard compounds (mentioned below),

824   was subjected to sonication in 500μL of ice-cold methanol. To this, an equal volume of ultrapure

825   water (LC/MS grade, Wako, Japan) and 0.4 volume of chloroform were added. The resulting

826   suspension was centrifuged at 15,000×g for 15 minutes at 4 °C. The aqueous phase was then

827   filtered using an ultrafiltration tube (Ultrafree MC-PLHCC, Human Metabolome Technologies,

828   Japan), and the filtrate was concentrated by nitrogen spraying (aluminum block bath with nitrogen

829   gas spraying system, DTU-1BN/EN1-36, TAITEC, Japan). The concentrated filtrate was dissolved

830   in 50μL of ultrapure water and utilized for IC-MS and LC-MS/MS analysis. Methionine sulfone

831   and 2-morpholinoethanesulfonic acid were employed as internal standards for cationic and anionic

832   metabolites, respectively. The recovery rate (%) of the standards in each sample measurement was

833   calculated to correct for the loss of endogenous metabolites during sample preparation.

834   **IC-MS metabolome analysis**

835 Anionic metabolites were detected using an orbitrap-type MS (Q-Exactive focus; Thermo Fisher

836 Scientific, USA) connected to a high-performance ion-chromatography (IC) system (ICS-5000+,

837 Thermo Fisher Scientific, USA) that allows for highly selective and sensitive metabolite

838 quantification through IC separation and Fourier transfer MS principle. The IC system included a

839 modified Thermo Scientific Dionex AERS 500 anion electrolytic suppressor, which converted the

840 potassium hydroxide gradient into pure water before the sample entered the mass spectrometer.

841 Separation was carried out using a Thermo Scientific Dionex IonPac AS11-HC column with a

842 particle size of 4μm. The IC flow rate was 0.25 mL/min, supplemented post-column with a makeup

843 flow of 0.18 mL/min MeOH. The potassium hydroxide gradient conditions for IC separation were

844 as follows: from 1 mM to 100 mM (0–40 min), to 100 mM (40–50 min), and to 1 mM (50.1–60

845 min), with a column temperature of 30 °C. The Q Exactive focus mass spectrometer was operated

846 in the ESI-negative mode for all detections. A full mass scan (m/z 70–900) was performed at a

847 resolution of 70,000. The automatic gain control target was set at 3×10^6 ions, and the maximum

848 ion injection time was 100ms. The source ionization parameters were optimized with a spray

849 voltage of 3 kV, and other parameters were as follows: transfer temperature, 320 °C; S-Lens level

850 = 50, heater temperature, 300 °C; sheath gas = 36, and Aux gas, 10.

851

852 **LC-MS/MS metabolome analysis**

853 Cationic metabolites were measured using liquid chromatography-tandem mass spectrometry (LC-

854 MS/MS). The LCMS-8060 triple-quadrupole mass spectrometer (Shimadzu corporation, Japan)

855 with an electrospray ionization (ESI) ion source was employed to perform multiple reaction

856 monitoring (MRM) in positive and negative ESI modes. The samples were separated on a

857 Discovery HS F5-3 column (2.1 mm I.D. x 150 mm L, 3μm particle, Sigma-Aldrich) using a step

858 gradient of mobile phase A (0.1% formate) and mobile phase B (0.1% acetonitrile) with varying

859 ratios: 100:0 (0-5 min), 75:25 (5-11 min), 65:35 (11-15 min), 5:95 (15-20 min), and 100:0 (20-25

860 min). The flow rate was set at 0.25 mL/min, and the column temperature was maintained at 40°C.

861 **Monoamine measurements by HPLC with electro chemical detector (ECD)**

862 For low concentration monoamine measurements, extracted tissue metabolites by abovementioned

863 protocol were injected with an autosampler (M-510, Eicom) into a HPLC unit (Eicom) coupled to

864 an ECD (ECD-300, Eicom). The samples were resolved on the Eicompak SC-5ODS column (φ3.0

865 x 150 mm, Eicom), using an isocratic mobile phase (5 mg/L EDTA-2Na, 220 mg/L sodium 1-

866 octanesulfonate in acetate/citrate buffer (0.1 M, pH 3.5)/MeOH (83:17, v/v)), at a flow rate of 0.5

867 mL/min and a column temperature of 25°C. At the ECD, analytes were subjected to oxidation

868 reactions within the ECD unit with WE-3G graphite electrode (applied potential is +750 mV

869 against an Ag/AgCl reference electrode). Resulting chromatograms were analyzed using the

870 software EPC-300 (Eicom).

871 **Lipidome analysis**

872 To extract total lipids, frozen tissues were mixed with 500 μL of 1-butanol/methanol (1:1, v/v)

873 containing 5 mM ammonium formate. The mixture was vortexed for 10 seconds, sonicated for 15

874 minutes in a sonic water bath, and then centrifuged at 16,000 × g for 10 minutes at 20°C. The

875 supernatant was transferred to a 0.2-mL glass insert with a Teflon insert cap for LC ESI-MS

876 analysis.

877

878 For lipidomic analysis, a Q-Exactive focus orbitrap mass spectrometer (Thermo Fisher Scientific,

879 San Jose, CA) was connected to an HPLC system (Ultimate3000, Thermo Fisher Scientific). The

880 samples were separated on a Thermo Scientific Accucore C18 column (2.1 × 150 mm, 2.6 μm)

881 using a step gradient of mobile phase A (10 mM ammonium formate in 50% acetonitrile and 0.1%

882 formic acid) and mobile phase B (2 mM ammonium formate in acetonitrile/isopropyl

883 alcohol/water, ratios of 10:88:2, v/v/v, with 0.02% formic acid). The gradient ratios used were

884 65:35 (0 min), 40:60 (0-4 min), 15:85 (4-12 min), 0:100 (12-21 min), 0:100 (21-24 min), 65:35

885 (24-24.1 min), and 100:0 (24.1-28 min) at a flow rate of 0.4 mL/min and a column temperature of

886 35°C.

887 The Q-Exactive focus mass spectrometer operated in both positive and negative ESI modes. It

888 performed a full mass scan (m/z 250-1100), followed by three rapid data-dependent MS/MS scans,

889 at resolutions of 70,000 and 17,500, respectively. The automatic gain control target was set at $1 \times$

890 10^6 ions, and the maximum ion injection time was 100 ms. The source ionization parameters

891 included a spray voltage of 3 kV, transfer tube temperature of 285°C, S-Lens level of 45, heater

892 temperature of 370°C, sheath gas at 60, and auxiliary gas at 20. The acquired data were analyzed

893 using LipidSearch software (Mitsui Knowledge Industry, Tokyo, Japan) for major phospholipids

894 (PLs). The search parameters for LipidSearch software were as follows: precursor mass tolerance

895 = 3 ppm, product mass tolerance = 7 ppm, and m-score threshold = 3.

896

897 **Visualizing noradrenaline distribution using MALDI-imaging mass spectrometry**

898 The tissue block was frozen and secured onto a disc using a cryoembedding medium (Super

899 Cryoembedding Medium, SECTION-LAB, Hiroshima, Japan), then equilibrated at -16°C in

900 cryostats (Leica Biosystems, Nussloch, Germany). Tissue sections, 8 µm thick, were cut and

901 mounted onto conductive indium-tin-oxide (ITO)-coated glass slides (Matsunami Glass Industries,

902 Osaka, Japan)., A solution of tetrafluoroborate salts of 2,4-diphenyl-pyrylium (DPP) (1.3 mg/mL

903 in methanol) for on-tissue derivatization of monoamines, and DHB-matrix (50 mg/mL in 80%

35

904   ethanol) were manually sprayed onto the tissue using an airbrush (Procon Boy FWA platinum; Mr.

905   Hobby, Tokyo). The manual spray was performed at room temperature, applying 40 μL/mm2 with

906   a distance of approximately 50 mm. The samples were analyzed using a linear ion trap mass

907   spectrometer (LTQ XL, Thermo Fisher Scientific). The raster scan pitch was set at 50 μm. Signals

908   of noradrenaline-DPP (m/z 384 > 232) were monitored with a precursor ion isolation width of m/z

909   1.0 and a normalized collision energy of 45%. Ion images were reconstructed using ImageQuest

910   1.1.0 software (Thermo Fisher Scientific).

911

912   **Core-body temperature measurement**

913   Animals were anesthetized with isoflurane, first at a rate of 2-3% and maintained at 0.5-2% in

914   oxygen during surgery. Mice were kept on a heating pad throughout surgery. Mice were injected

915   with buprenorphine and bupivacaine as pre-emptive analgesia. A small ventral incision of 1cm

916   was made after clipping hair and disinfection with betadine and 70% ethanol. DST nano-T

917   temperature loggers (Star Oddi) were placed in the peritoneal cavity, and abdominal muscle and

918   skin were sutured closed. Post-surgery, mice were singly housed and provided with Meloixcam

919   for 48 hours. After 7 days, sutures were removed. 10 days after surgery, mice were started on

920   CTRL or CysF diet, and loggers were removed for data collection after euthanization. Loggers

921   were programmed to take temperature readings every 30 minutes.

922   **Metabolic cages**

923   The energy expenditure (EE), respiratory exchange ratio (RER), activity, food intake of mice were

924   monitored using the TSE PhenoMaster System (V3.0.3) Indirect Calorimetry System. Each mouse

925   was housed in individual chambers for 3 days for acclimation and switched to experimental diet

926   for 6 days. Each parameter was measured every 30 min. EE and RER were calculated based on

927   the oxygen consumption (O_2) and carbon dioxide production (CO_2). Mouse activity was detected

36

928   by infrared sensors, and food intake and water consumption were measured via weight sensors on

929   food and water dispensers located in the cage.

930   **EchoMRI**

931   The parameters of body composition were measured in vivo by magnetic resonance imaging

932   (EchoMRI; Echo Medical Systems). The amount of fat mass, lean mass and free water were

933   measured by the analysis. For the analysis, each mouse was placed in an acrylic tube with breathing

934   holes and the tube was inserted in the MRI machine. The analysis per mouse takes approximately

935   90 sec and automatically calculated numerical results were analyzed.

936   **Climate chambers**

937   Mice were acclimated in climate chambers (model 7000-10, Caron) at either 30°C or 20°C, with

938   humidity maintained at 50% under 12 h light/dark cycles. After one week acclimation, mice were

939   switched to either CTRL or CysF diet for 6 days, while maintained in the climate chambers. Mice

940   were handled daily to measure body weight.

941   **Feces bomb calorimetry**

942   Feces were collected daily over the course of CTRL or CysF feeding. Samples were dried for 72

943   hours. Fecal bomb calorimetry was performed at UT Southwestern Medical Center Metabolic

944   Phenotyping Core (Dallas, TX, USA) using a Parr 6200 Isoperibol Calorimeter equipped with a

945   6510 Parr Water Handling.

946   **Serum measurements**

947   After blood collection by cardiac puncture, samples were allowed to clot for 2 hours. Serum was

948   collected after centrifugation. FGF21 and GDF15 levels in the serum were measured by ELISA

949   (R&D). Cysteine levels were determined by competitive EIA (LS-Bio). Glycerol levels were

950   determined by colorimetric assay (Sigma Aldrich).

951 **β-3 adrenergic receptor inhibition**

952 Mice were administered twice daily L748337 (Santa Cruz Biotechnology) (5mg/kg) by i.p

953 injection. Mice were weighed daily and assessed for their health.

954 **Histology**

955 Tissues were collected in 10% formalin, embedded in paraffin and sectioned into 5um thick

956 sections. Tissues were stained with hematoxylin and eosin (H&E) or stained for UCP1 (Abcam)

957 and Goat anti-rabbit HRP (DAKO) and developed for color using Abcam DAB substrate kit.

958 **Animal preparation for BIRDS Temperature Analysis**

959 The animals were anesthetized with 3% isoflurane in an induction chamber and then kept at 2-3%

960 during surgery. The animal was laid back on a microwaveable heating pad. Prior to incision, a

961 single dose of bupivacaine was given for analgesia. A 1-2 cm midline incision was made on the

962 neck to expose the jugular vein. Another small incision (<1 cm) was made at the back of the neck.

963 A sterile polyurethane or silicone catheter with a metal guide was inserted from the back of the

964 neck, where the vascular port was fixed to the jugular vein. Prior to implantation the port and the

965 catheter were flushed with heparinized saline (25 IU/ml). The jugular vein was catheterized toward

966 the heart. The skin was closed with surgical sutures after application of triple antibiotic ointment

967 and the vascular port was fixed. The duration of the surgical procedure was 15-20 min.

968 **MR data acquisition.**

969 TmDOTMA$^-$ was purchased from Macrocyclics (Plano, TX, USA). Temperature mapping with

970 BIRDS was performed on a 9.4T Bruker scanner (Billerica, MA). The respiration rate was

971 monitored during the entire duration of the experiment. A 200mM TmDOTMA$^-$ solution was

972 infused at a rate of 60 to 80 µl/h for 1 to 2 hours. The infusion rate was adjusted according to

973 animal physiology. The T$_2$ weighted magnetic resonance (MR) images were acquired with an FOV

974   of 23x23mm^2, 128x128 matrix, 23 slices of 0.5mm thickness, TR=3s and TE=9ms. The extremely

975   short T_1 and T_2 relaxation times (<5ms) of the TmDOTMA$^-$ methyl group allowed ultrafast

976   temperature mapping with BIRDS using 3D chemical shift imaging (CSI) acquisition with a short

977   TR (10ms) and wide bandwidths (±150ppm). Temperature mapping with BIRDS was started

978   immediately after detection of global MR signal of TmDOTMA$^-$ methyl group, at about 1 hour

979   after the start of the infusion. The CSI was acquired using a FOV of 23x15x23mm^3, 809 spherical

980   encoding steps, 21min acquisition, and reconstructed to 23x15x23, with a voxel resolution of

981   1x1x1mm^3. Selective excitation of the TmDOTMA$^-$ methyl group was achieved using a single

982   band 200µs Shinnar-Le Roux (SLR) RF pulse. The MR spectrum in each voxel was line broadened

983   (200 Hz) and phased (zero-order) in Matlab (MathWorks Inc., MA, USA), and the corresponding

984   temperature T_c was calculated from the chemical shift δ_{CH_3} of the TmDOTMA$^-$ methyl group

985   according to

986
$$T_c = a_0 + a_1(\delta_{CH_3} - \delta_0) + a_2(\delta_{CH_3} - \delta_0)^2 \qquad [1]$$

987   where δ_0 = -103.0 ppm and the coefficients $a_0 = 34.45 \pm 0.01$, $a_1 = 1.460 \pm 0.003$ and $a_2 = 0.0152$

988   ± 0.0009 were calculated from the linear least-squares fit of temperature as a function of chemical

989   shift δ_{CH_3} (reference below). Statistical analysis was done using Student's t-test with two tails,

990   with p<0.05 used as a cutoff for significance.

991

992   **In vivo spin trapping and Electron Paramagnetic Resonance (EPR) spectroscopy**

993   POBN (α-(4-Pyridyl-1-oxide)-N-t-butylnitrone, Enzo) was used for spin trapping; POBN was

994   dissolved in saline and administered i.p. at 500 mg/kg body weight. Tissue samples (VFAT, SFAT

995   and BAT) were collected 45 minutes post-injection, immediately frozen in liquid nitrogen, and

996   stored at −80°C until EPR measurements. Lipid extraction was performed using

997   chloroform/methanol (2/1) (Folch-extraction) as described previously[59]. All EPR spectra were

39

998   recorded in a quartz flat cell using an X-band EMX plus EPR Spectroscope (parameters: 3,480 ±

999   80 G scan width, 105 receiver gain, and 20 mW microwave power; time constant: 1,310 ms;

1000   conversion time: 655 ms).

Aconitase activity

1002   Aconitase activity was measured with Aconitase Assay kit (Cayman). Freshly collected SFAT and

1003   VFAT samples were measured at 500 μg total protein/mL, and BAT samples were measured at

1004   100 μg total protein/mL. All results were normalized to 500 μg/mL total protein concentration.

1005   Standard protocols provided with the kits was followed.

***In vitro* adipocyte differentiation**

1007   Stromal vascular fraction from visceral depots of $Cth^{-/-}$ was isolated as previously described. Cells

1008   were plated in growth medium (DMEM supplemented with 10% FBS and 1% Penicillin-

1009   Streptomycin) and expanded for 3-5 days. Adipocyte differentiation was induced with growth

1010   medium supplemented with insulin (5μg/ml), rosiglitazone (1μM), iso-butyl-methylxanthine

1011   (0.5mM) and dexamethasone (1μM) for 48hrs. Cells were maintained on differentiation medium

1012   containing insulin (5μg/ml) and rosiglitazone (1μM) for 96hr. Fully differentiated cells were then

1013   treated with various concentrations of Cystine (0-200μM) for 48hr, in cystine and methionine-free

1014   DMEM (Gibco) supplemented with 10% dialyzed FBS, 1% Penicillin-Streptomycin and 200μM

1015   methionine.

Quantification and statistical analysis

1017   Statistical differences between groups were calculated by unpaired t-tests. For comparing groups

1018   over time, mice were individually tracked and groups were compared using 2-way ANOVA with

1019   Sidak's correction for multiple comparisons. For all experiments a p-value of p≤0.05 was

1020   considered significant.

Figure 1, Lee et al

1021

41
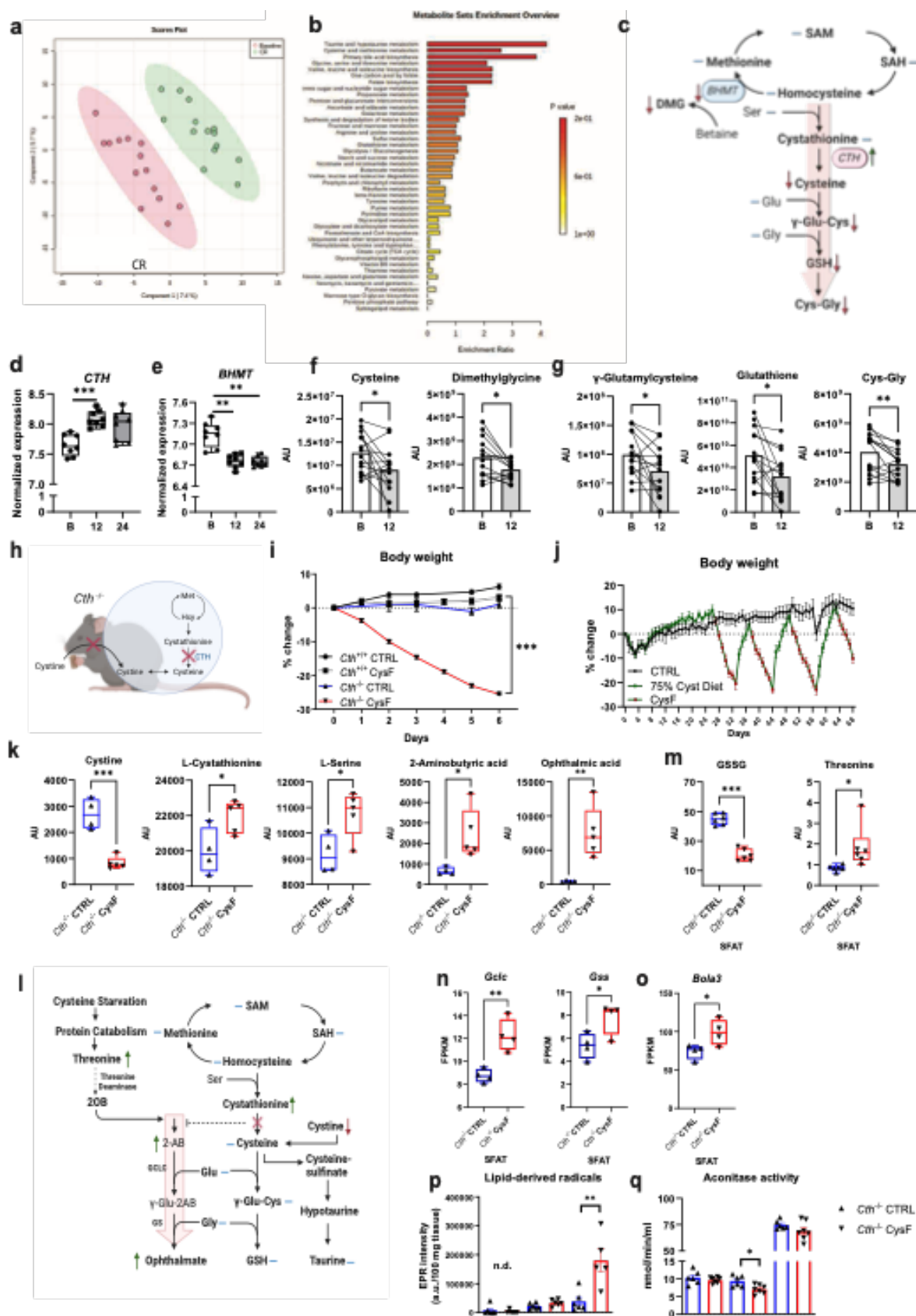
Figure 1: Cysteine deficiency induces weight-loss. a) Principal component analysis of the metabolome of subcutaneous adipose depots (SFAT) of healthy individuals at baseline and after 12 months of caloric restriction (CR) (n=14). b) Metabolite set enrichment analysis shows that compared to baseline, one year of CR in humans activates TSP, with increased cysteine and taurine metabolism. c) Schematic summary of TSP and metabolites from baseline to one year CR, measured in human SFAT. Blue lines indicate unchanged metabolites, green and red arrows indicate significantly increased or decreased metabolites or genes respectively, via paired t-test (p<0.05). d-e) Normalized expression of changes in *CTH*, and *BHMT* in human SFAT at baseline, after 12 months, and 24 months of CR. Adjusted p-values were calculated in the differential gene expression analysis in a separate cohort from metabolome analyses in the CALERIE-II trial (n=8). f-g) Change in metabolites in human SFAT at baseline (B) and 12 months of CR. Significance was calculated using paired t-tests (n=14). AU: arbitrary unit. h) Mouse model used to achieve cysteine deficiency utilizing *Cth*$^{-/-}$ mice fed a Cystine free (CysF) diet. i) Male *Cth*$^{+/+}$ and *Cth*$^{-/-}$ mice were fed control (CTRL) or CysF diets for 6 days (n=5 *Cth*$^{+/+}$ CTRL, n=12 *Cth*$^{+/+}$ CysF, n=8 *Cth*$^{-/-}$ CTRL, n=17 *Cth*$^{-/-}$ CysF, 3 experiments pooled). Percent body weight represented over 6 days of diet. j) *Cth*$^{-/-}$ mice were fed purified control diet (black line) or a diet containing 75% cysteine (green line) alternately switched to CysF diet (green line with red dots n = 6/group). k) Box plots of metabolites involved in TSP in the serum of *Cth*$^{-/-}$ mice fed CTRL or CysF diet for 6 days (n=4 *Cth*$^{-/-}$ CTRL, n=5 *Cth*$^{-/-}$ CysF). l) Schematic summary of changes in the metabolites in the serum of *Cth*$^{-/-}$ mice fed CTRL or CysF diet for 6 days. Blue lines represent measured, but unchanged metabolites, red and green arrows indicate significantly decreased or increased metabolites, respectively (p<0.05). m) Box plots of GSSG and threonine quantification in the SFAT of *Cth*$^{-/-}$ mice fed CTRL or CysF diet for 6 days (n=6/group). n-o) RNA-seq based expression of (n) *Gclc*, *Gss* and (o) *Bola3* in the

42

1045   SFAT of $Cth^{-/-}$ mice fed with CTRL or CysF for 6 days. p) Analysis of EPR spectra of POBN-lipid

1046   radical adducts measured in Folch extracts of VFAT, SFAT and BAT tissues from $Cth^{-/-}$ mice fed

1047   with CTRL or CysF diet for 5 days, normalized to 100 mg (n.d=not detectable, n=5-6/group). q)

1048   Aconitase activity determined in VFAT, SFAT and BAT tissues from $Cth^{-/-}$ fed with CTRL or

1049   CysF diet for 5 days (n=6-7/group). Data are represented as mean ± SEM. Unless mentioned,

1050   differences were determined with unpaired t-tests (*p<0.05, **p<0.01, ***p<0.001).
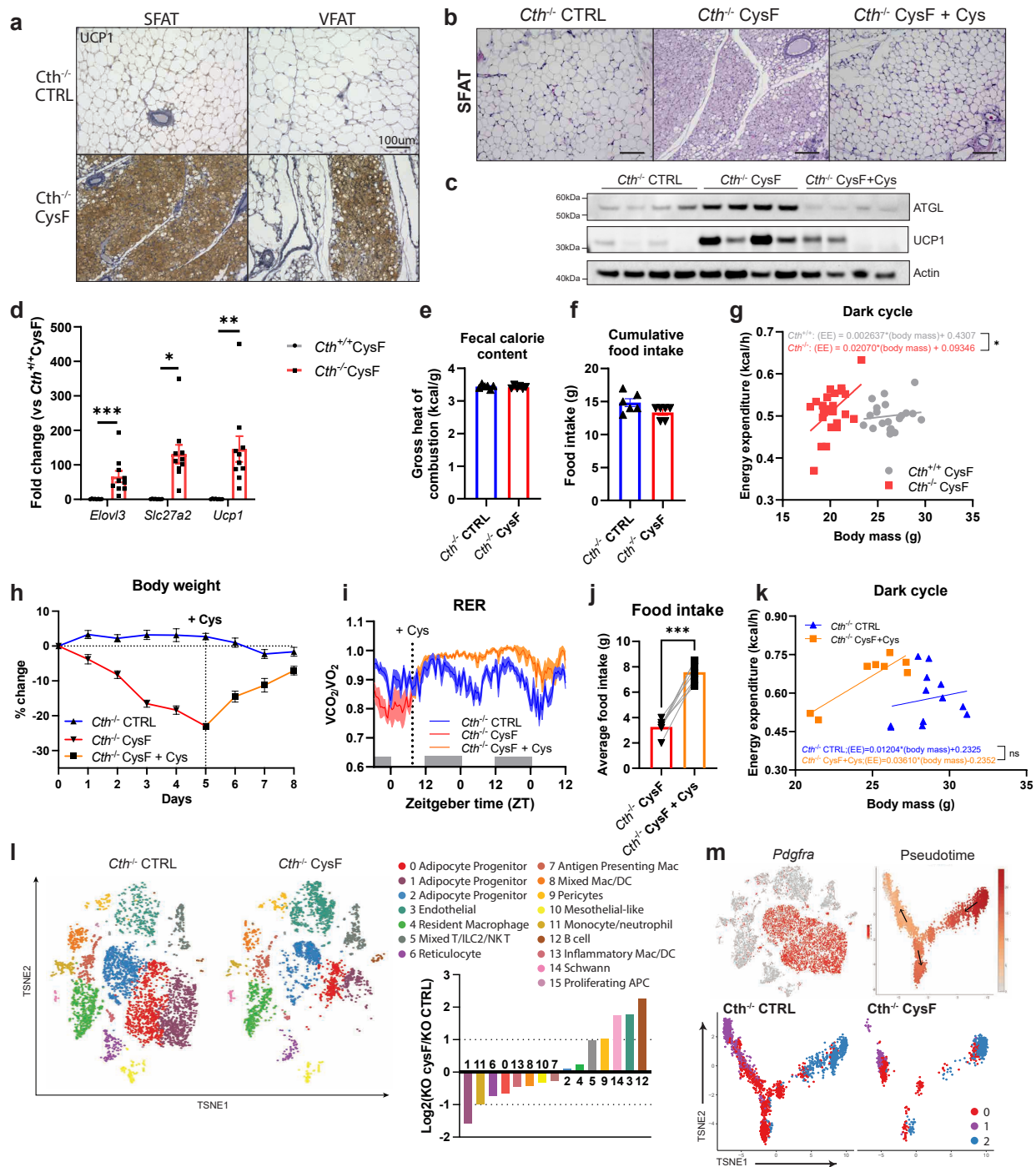
Figure 2, Lee et al

Figure 2: Cysteine depletion induces browning of adipose tissue. a) Representative images of subcutaneous (SFAT) and visceral (VFAT) fat sections stained for UCP1 from $Cth^{-/-}$ mice fed CTRL or CysF diet for 6 days (scale bar=100um). b) Representative H&E-stained sections of

44

1055   SFAT of $Cth^{-/-}$ mice fed CTRL or CysF diet for 6 days or CysF diet followed by Cys-supplemented

1056   diet for 4 days (CysF+Cys) (scale bar=100 μm). c) Western blot detection of ATGL and UCP1 in

1057   SFAT from $Cth^{-/-}$ mice after 6 days of CTRL or CysF diet or Cys supplementation after CysF-

1058   induced weight loss. Actin is used as a loading control. d) qPCR analysis of thermogenic genes in

1059   SFAT of $Cth^{+/+}$ and $Cth^{-/-}$ mice fed CysF diet for 6 days (n=8 $Cth^{+/+}$ and n=10 $Cth^{-/-}$). e) Fecal

1060   calorie content and f) cumulative food intake of $Cth^{-/-}$ mice fed CTRL or CysF diet for 4 days

1061   (n=6/group). g) Linear regression analysis of energy expenditure against body mass during dark

1062   cycle at 4, 5 days of weight loss (n=10 $Cth^{+/+}$ CysF and n=12 $Cth^{-/-}$ CysF). h) Percent body weight

1063   change of $Cth^{-/-}$ mice fed with CTRL diet or CysF diet (red line) for 5 days and then switched to

1064   Cys-containing diet (orange line) for 3 days (n=6/group). i) Respiratory exchange ratio (RER)

1065   measured in metabolic cages, of $Cth^{-/-}$ mice fed with CTRL diet or Cys-containing diet after CysF

1066   induced weight loss (n=4-6/group). j) Average food intake of $Cth^{-/-}$ mice fed with CysF diet and

1067   then switched to Cys-containing diet for 2 days (n=7/group). Significance was measured with

1068   paired t-test. k) Linear regression analysis of energy expenditure against body mass during dark

1069   cycle of $Cth^{-/-}$ mice fed with CTRL or Cys-supplemented diet after CysF induced weight loss (n=4-

1070   6/group), average values of the first two nights after diet switch. l) t-SNE plot of scRNAseq

1071   showing cluster identities from SFAT stromal vascular fraction from $Cth^{-/-}$ mice fed CTRL or CysF

1072   diet at day 4 of weight-loss and bar chart showing population fold changes in relative abundance

1073   of each cluster comparing $Cth^{-/-}$ CysF vs. $Cth^{-/-}$ CTRL. m) t-SNE plot displaying $Pdgfra$ expression

1074   in red across all populations and monocle analysis of clusters 0, 1, and 2, with coloring by

1075   pseudotime to show right most cluster giving rise to two separate clusters. Each cluster represented

1076   by color in $Cth^{-/-}$ CTRL and $Cth^{-/-}$ CysF. Data are expressed as mean±SEM. Statistical differences

1077   were calculated by 2-way ANOVA with Sidak's correction for multiple comparisons or unpaired

1078   t-test (*p<0.05, **p<0.01, ***p<0.001).
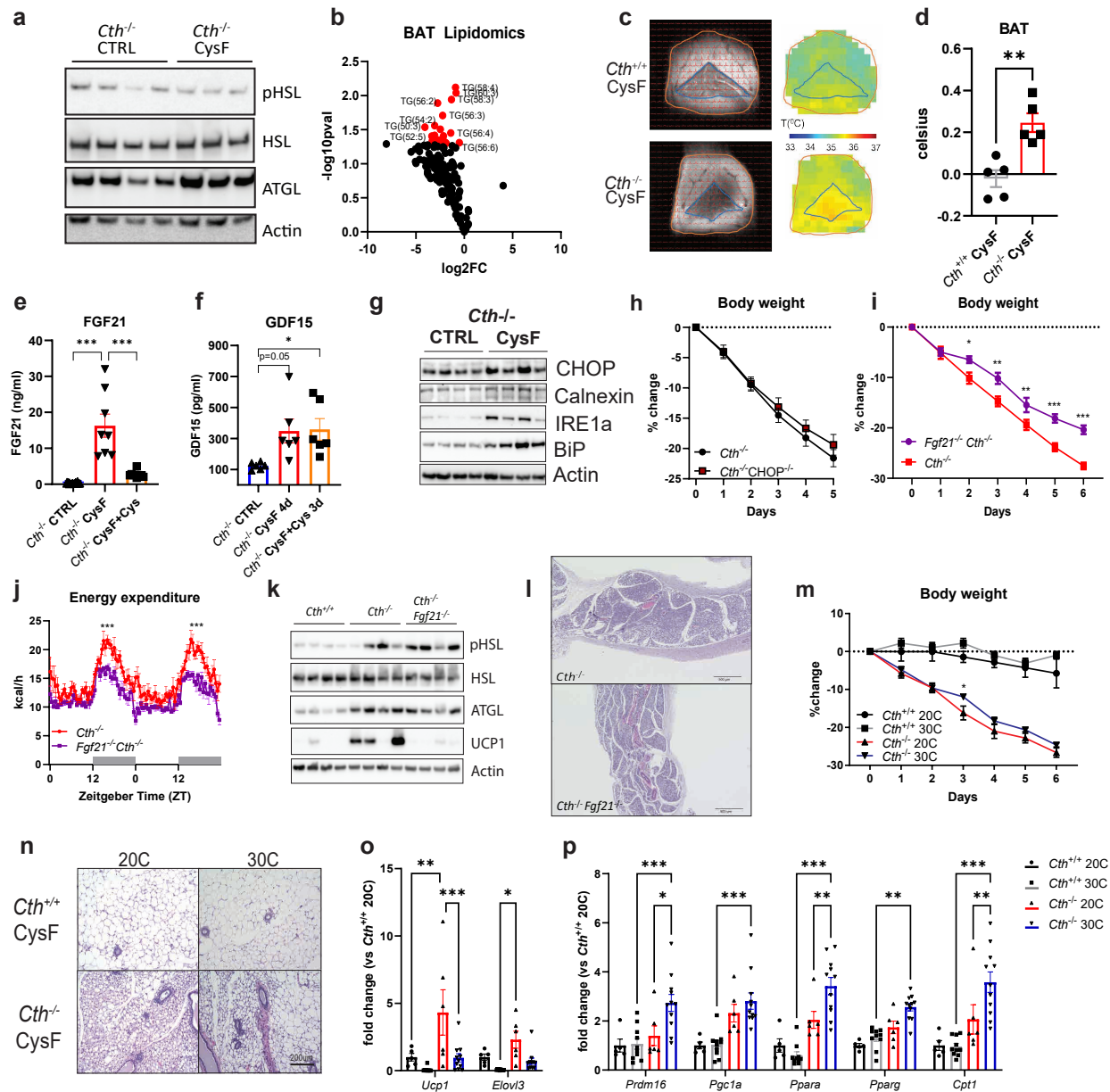
1079   *Figure 3, Lee et al*

1080   **Figure 3: FGF21 is partially required for cysteine-restriction mediated weight-loss.** a)

1081   Western blot detection of lipolysis regulators pHSL, HSL and ATGL in SFAT from $Cth^{-/-}$ mice

1082   after 6 days of CTRL or CysF diet, actin is used as loading control. b) Volcano plot of lipid species

1083   of BAT showing fold change of triglycerides in $Cth^{-/-}$ mice fed CTRL or CysF diet. c) *in vivo*

1084   measurement of BAT temperature by BIRDS imaging and d) quantification of local temperature

1085   differences in BAT compared to surrounding tissue in $Cth^{+/+}$ and $Cth^{-/-}$ mice on CysF diet for 6

1086   days (n=5/group). e) Serum FGF21 quantification in $Cth^{-/-}$ CTRL (n=23), $Cth^{-/-}$ CysF for 6 days

1087   (n=8) and Cth$^{-/-}$ CysF followed with 4 days of Cys supplementation (n=10). f) Serum GDF15

1088   concentrations in $Cth^{-/-}$ CTRL, $Cth^{-/-}$ CysF for 4 days and Cth$^{-/-}$ CysF followed with 3 days of Cys

1089   supplementation (n=6/group). g) Immunoblot analysis of CHOP, Calnexin, IRE1a, BiP in the liver

1090   of $Cth^{-/-}$ mice fed with CTRL or CysF diet at day 6. Actin was used as loading control. h)

1091   Percentage body weight change of $Cth^{-/-}$ and $Cth^{-/-}$CHOP$^{-/-}$ mice fed with CysF diet for 5 days

1092   (n=17 $Cth^{-/-}$ and n=15 $Cth^{-/-}$CHOP$^{-/-}$). i) Percentage body weight change of $Cth^{-/-}$ and $Fgf21^{-/-}Cth^{-/-}$

1093   mice fed with CysF diet for 5 days (n=13 $Cth^{-/-}$ and n=18 $Fgf21^{-/-}Cth^{-/-}$). j) Energy expenditure

1094   measured in metabolic cages of $Cth^{-/-}$ and $Cth^{-/-}$ $Fgf21^{-/-}$ mice on days 3-4 of CysF diet (n=5/group).

1095   k) Immunoblot analysis of pHSL, HSL, ATGL, and UCP1 in SFAT of $Cth^{+/+}$, $Cth^{-/-}$ and $Cth^{-/-}Fgf21^{-/-}$

1096   mice fed CysF diet for 6 days. l) Representative H&E stained SFAT sections of $Cth^{-/-}$ and $Fgf21^{-/-}Cth^{-/-}$

1097   mice after 6 days of CysF diet (scale bar=500um). m-p) $Cth^{+/+}$ and $Cth^{-/-}$ mice were fed with

1098   CysF diet and housed at 20°C or 30°C for 6 days. m) Percentage body weight change (n=3 $Cth^{+/+}$

1099   20°C, n=4 $Cth^{+/+}$ 30°C, n=4 $Cth^{-/-}$ 20°C, n=5 $Cth^{-/-}$ 30°C), n) representative images of H&E staining

1100   of SFAT sections (scale bar=200um) and o-p) qPCR analysis of thermogenic markers (n=5 $Cth^{+/+}$

1101   20°C, n=10 $Cth^{+/+}$ 30°C, n=6 $Cth^{-/-}$ 20°C, n=11 $Cth^{-/-}$ 30°C). Data are expressed as mean±SEM.

1102   Statistical differences were calculated by one-way ANOVA with Tukey's correction for multiple

1103   comparisons or 2-way ANOVA with Sidak's correction for multiple comparisons or unpaired t-

1104   test (*p<0.05, **p<0.01, ***p<0.001).
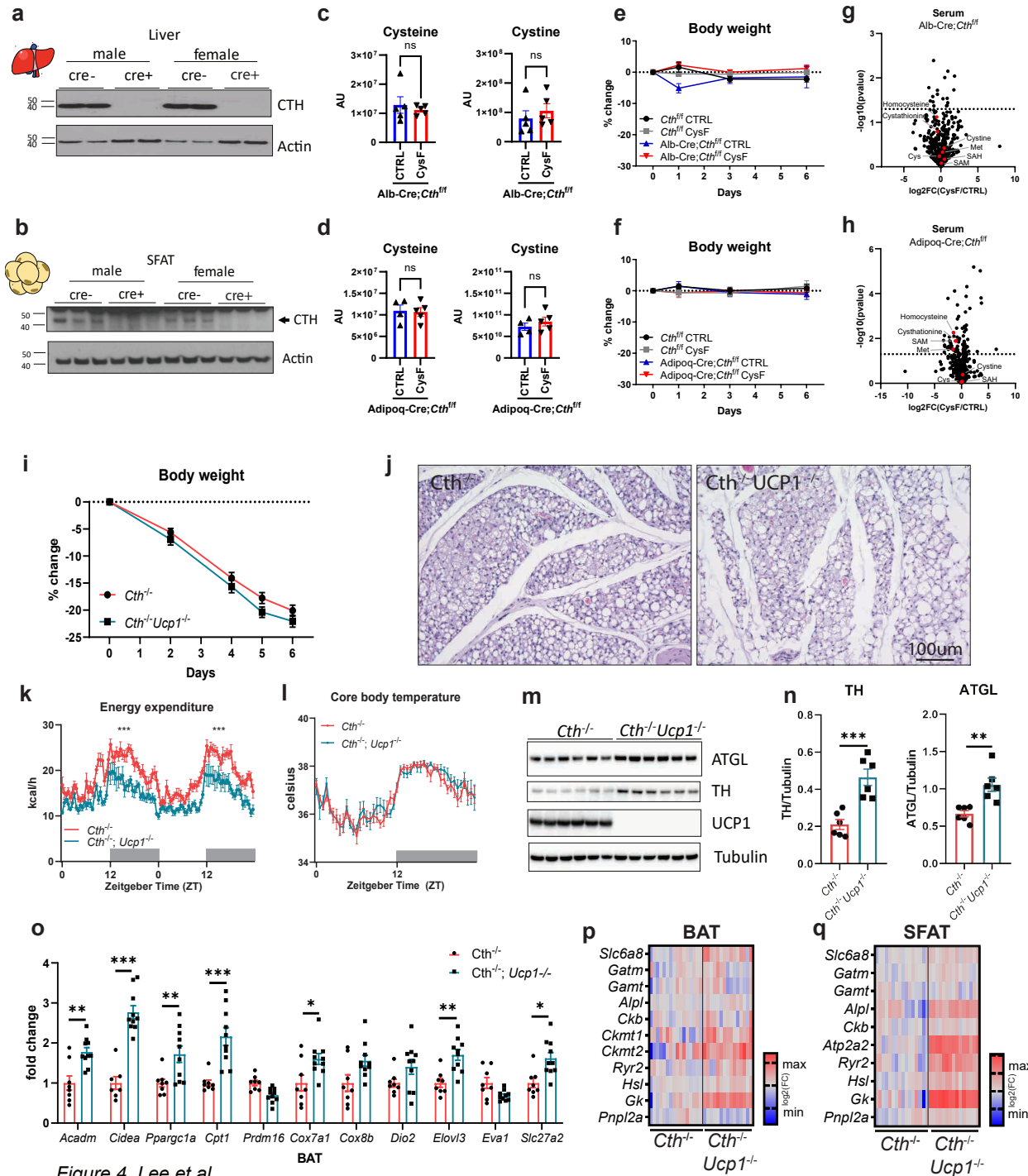
1105   *Figure 4, Lee et al*

Figure 4: Global cysteine deficiency induced adipose browning is UCP1 independent. a)

Immunoblot analyses of CTH in the liver of male and female *Cth*^f/f^ Alb:Cre^-^ or Alb: Cre^+^ mice. d)

Western blot detection of CTH in the SFAT of male and female *Cth*^f/f^ Adipoq:Cre^-^ or Adipoq:Cre^+^

1109   mice. c-d) Serum cysteine and cystine determined by LC-MS/MS in c) Alb:Cre⁺*Cth*ᶠ/ᶠ mice and d)

1110   Adipoq:Cre;*Cth*ᶠ/ᶠ mice after 5 days of CTRL or CysF diet (n=4-5/group). AU: arbitrary units. e-f)

1111   Percentage body weight changes of e) Alb-Cre;*Cth*ᶠ/ᶠ mice and f) Adipoq-Cre;*Cth*ᶠ/ᶠ mice after 5

1112   days of CTRL or CysF diet (n=4-5/group). g-h) Volcano plot of serum metabolites identified by

1113   LC-MS/MS in g) Alb-Cre;*Cth*ᶠ/ᶠ mice and i) Adipoq-Cre;*Cth*ᶠ/ᶠ mice after 5 days of CTRL or CysF

1114   diet (n=4-5/group). Transsulfuration pathway related metabolites are highlighted in red. Cys:

1115   cysteine. Met: methionine. SAH: S-adenosyl homocysteine. SAM: S-adenosyl methionine. i-k)

1116   *Cth*⁻/⁻ and *Cth*⁻/⁻ *Ucp*1⁻/⁻ mice were fed a CysF diet for 6 days (n=8/group). i) Percent body weight

1117   change over 6 days of diet. j) Representative H&E histology images of SFAT after 6 days of diet.

1118   k) Energy expenditure measured in metabolic cages on days 4 and 5 of CysF diet. l) Core body

1119   temperatures (CBT) measured in the peritoneal cavity by implantation of Star-Oddi loggers over

1120   6 days of diet in male *Cth*⁻/⁻ and *Cth*⁻/⁻ *Ucp1*⁻/⁻ mice fed CysF diet. Recordings were taken every

1121   30min and representative day 4 is plotted (n=7 *Cth*⁻/⁻, n=5 *Cth*⁻/⁻ *Ucp1*⁻/⁻). m) Immunoblot staining

1122   of ATGL, TH, and UCP1 in BAT of *Cth*⁻/⁻ and *Cth*⁻/⁻ *Ucp1*⁻/⁻ fed a CysF diet for 6 days and n)

1123   quantification using tubulin as loading control. o) Thermogenic markers gene expression analysis

1124   in BAT of *Cth*⁻/⁻ and *Cth*⁻/⁻ *Ucp1*⁻/⁻ mice fed a CysF diet for 6 days, measured by qPCR (n=8 *Cth*⁻/⁻,

1125   n=10 *Cth*⁻/⁻ *Ucp1*⁻/⁻). p-q) Heatmaps of gene expression of genes involved in creatine, calcium and

1126   lipid futile cycles in p) BAT and q) SFAT of *Cth*⁻/⁻ and *Cth*⁻/⁻ *Ucp1*⁻/⁻ mice fed a CysF diet for 6

1127   days (n=15-16/group), quantified by qPCR. Data are expressed as mean±SEM. Statistical

1128   differences were calculated by 2-way ANOVA with Sidak's correction for multiple comparisons,

1129   or by unpaired t-test (*$p<0.05$, **$p<0.01$, ***$p<0.001$).
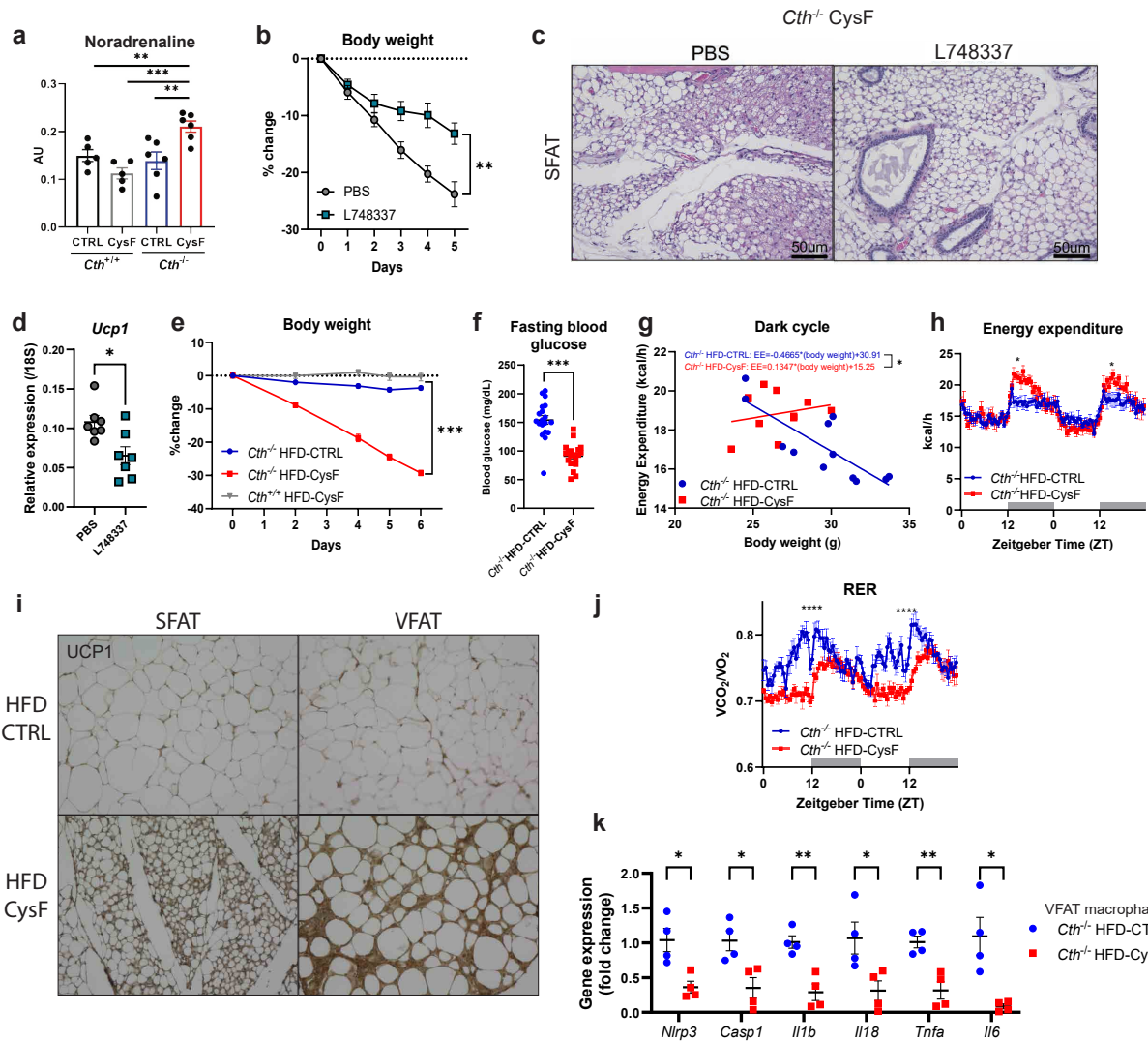
1130   *Figure 5, Lee et al*

Figure 5: Cysteine-elimination induced browning and weight loss requires noradrenergic signaling. a) Measurement of noradreanaline by orbitrap MS/MS in the SFAT of $Cth^{+/+}$ and $Cth^{-/-}$ fed 6 days of CTRL or CysF diet (n=5 $Cth^{+/+}$ CTRL, n=5 $Cth^{+/+}$ CysF, n=6 $Cth^{-/-}$ CTRL, n=6 $Cth^{-/-}$ CysF). b-d) $Cth^{-/-}$ mice were fed with CysF diet for 5 days and treated daily with a β-3 adrenergic receptor antagonist (L748337) or vehicle (PBS) (n=7/group). b) Percentage body weight change. c) Representative images of hematoxylin and eosin (H&E) staining of SFAT sections (scale bar=50um). d) qPCR gene expression of *Ucp1* in BAT depots. e-j) $Cth^{-/-}$ mice that had been fed a high fat diet (HFD) for 12 weeks were switched to a HFD containing (HFD-CTRL) or lacking

50

1139   cystine (HFD-CysF). e) Percentage body weight change after switching to HFD-CysF diet (n=6

1140 $Cth^{-/-}$ HFD-CTRL, n=5 $Cth^{-/-}$ HFD-CysF and n=5 $Cth^{+/+}$ HFD-CysF). f) Fasting blood glucose

1141   measured 1 week post diet switch ($Cth^{-/-}$ HFD-CTRL n=19, $Cth^{-/-}$ HFD-CysF, n=20). g) Linear

1142   regression analysis of energy expenditure (EE) against body mass during dark cycle and (h) EE of

1143 $Cth^{-/-}$ mice fed with HFD-CTRL or HFD-CysF, average values of nights 4 and 5 of diet switch

1144   (n=6 $Cth^{-/-}$ HFD-CTRL, n=5 $Cth^{-/-}$ HFD-CysF). i) Representative histological sections of SFAT

1145   and VFAT stained for UCP1, 6 days after diet switch. j) Respiratory exchange ratio (RER)

1146   measured in metabolic chambers on days 4 and 5 of diet switch (n=6 $Cth^{-/-}$ HFD-CTRL, n=5 $Cth^{-/-}$

1147 $^{-/-}$ HFD-CysF). k) Q-PCR analysis of inflammatory genes in VFAT macrophages of $Cth^{-/-}$ mice after

1148   diet switch to HFD-CTRL or HFD-CysF (n=4/group). Data are expressed as mean±SEM.

1149   Statistical differences were calculated by 2-way ANOVA with Sidak's correction for multiple

1150   comparisons, or by unpaired t-test (*p<0.05, **p<0.01, ***p<0.001).
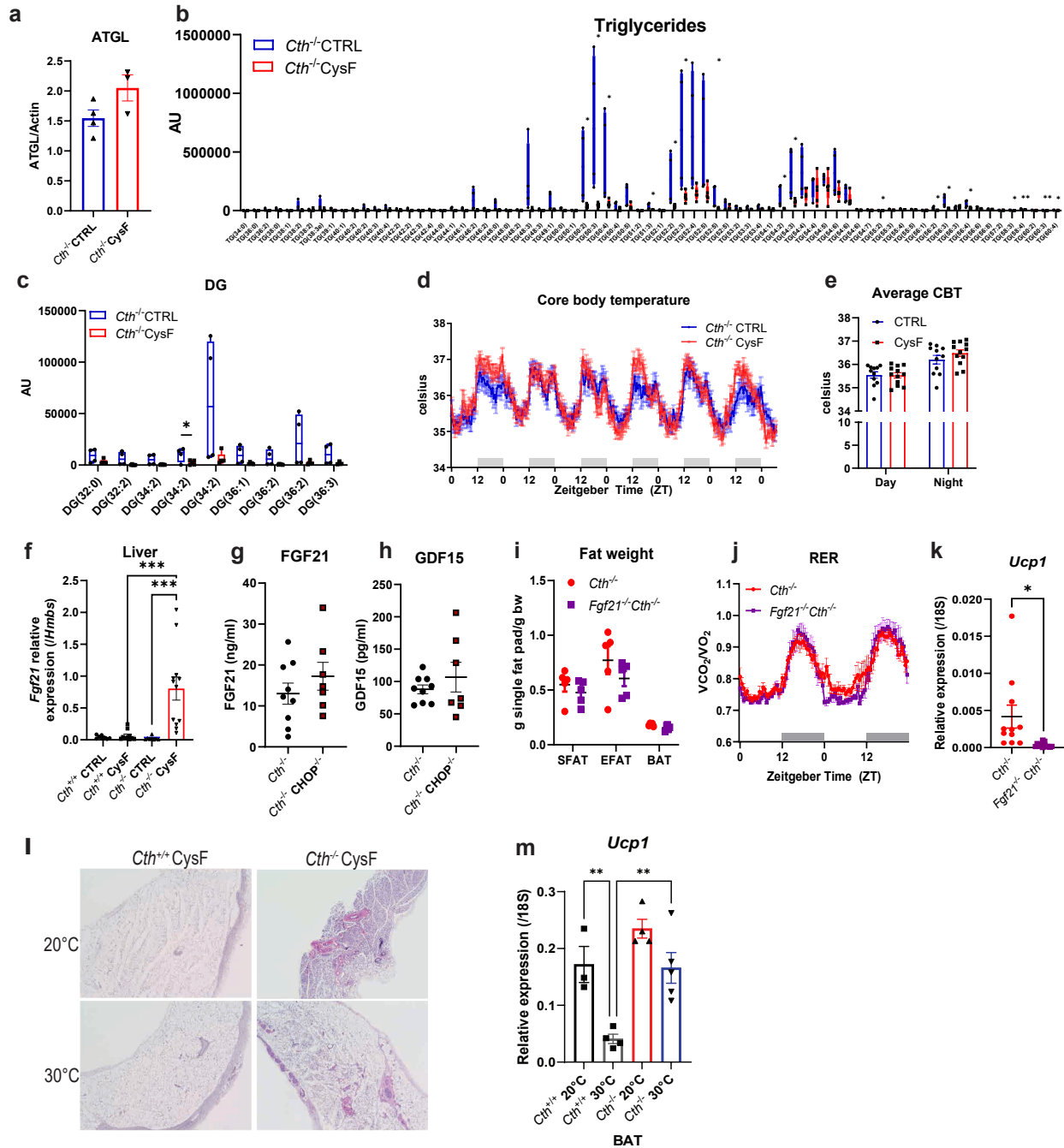
Extended Data Figure 1, Lee et al
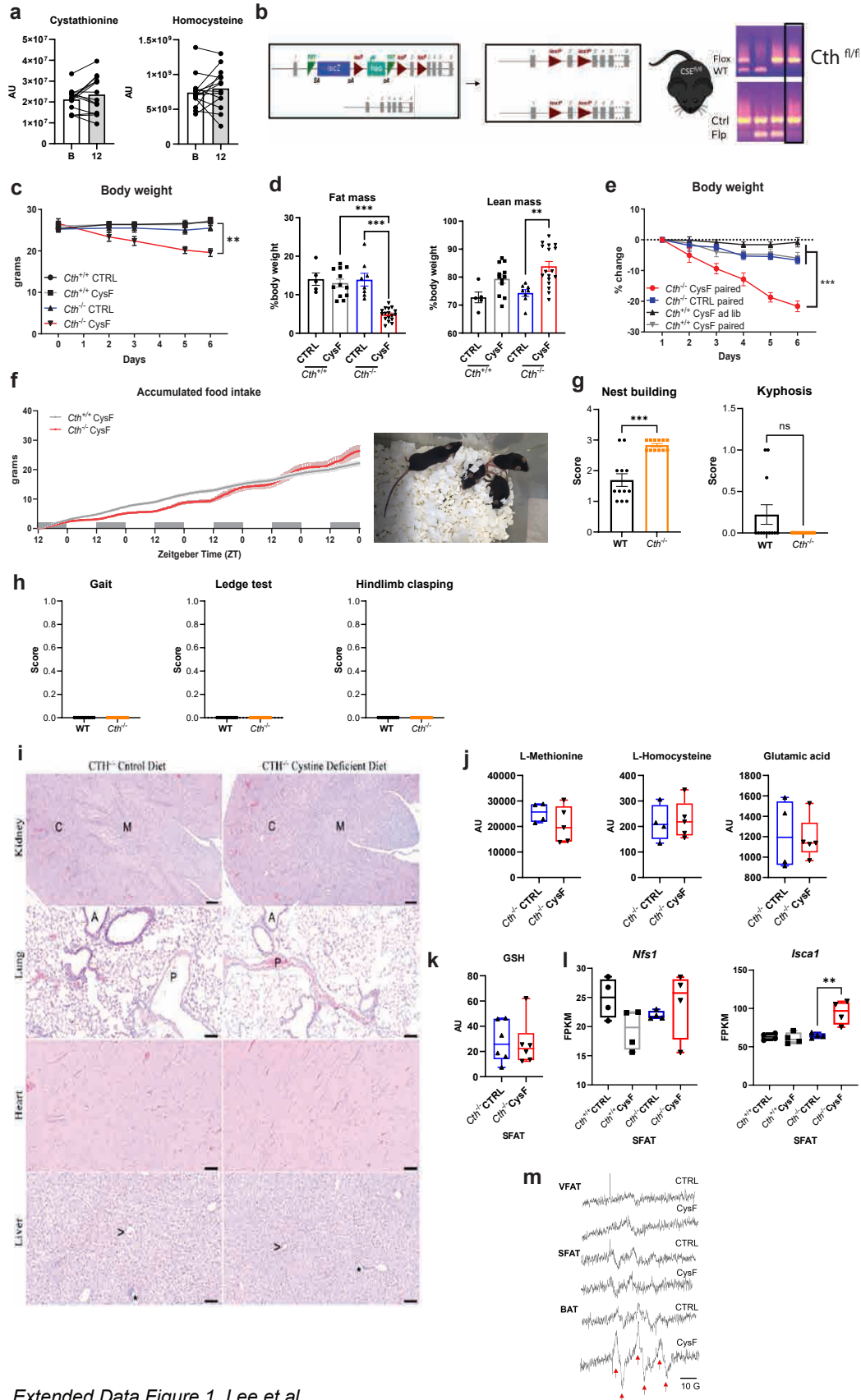
1152 **Extended Data Figure 1: Cysteine depletion induces weight-loss in mice without overt**

1153 **pathology**. a) Cystathionine and homocysteine measurements by MS/MS in human SFAT at

1154 baseline (B) and after 12 months of caloric restriction (n=14). AU: arbitrary units. b) Schematic of

1155 $Cth^{-/-}$ and $Cth^{fl/fl}$ mice generation (KOMP construct) used to cross to either Alb:cre or Adipoq:cre.

1156 c) Body weight of $Cth^{+/+}$ and $Cth^{-/-}$ mice fed with CTRL or CysF diet for 6 days (n=5 $Cth^{+/+}$ CTRL,

1157 n=6 $Cth^{+/+}$ CysF, n=4 $Cth^{-/-}$ CTRL, n=5 $Cth^{-/-}$ CysF). d) Fat mass and lean mass measured by

1158 EchoMRI of male $Cth^{+/+}$ and $Cth^{-/-}$ after 6 days of CTRL or CysF diet (n=5 $Cth^{+/+}$ CTRL, n=12

1159 $Cth^{+/+}$ CysF, n=8 $Cth^{-/-}$ CTRL, n=17 $Cth^{-/-}$ CysF). e) $Cth^{+/+}$ and $Cth^{-/-}$ mice were fed ad libitum (ad

1160 lib) or pair fed CTRL or CysF diet (n=4 $Cth^{+/+}$CysF ad lib, n=5 $Cth^{+/+}$CysF pair fed, n=7 $Cth^{-/-}$

1161 CTRL pair fed, n=5 $Cth^{-/-}$ CysF pair fed). Percentage body weight change over 6 days of diet. f)

1162 Accumulated food intake of $Cth^{+/+}$ and $Cth^{-/-}$ mice over 6 days of CysF feeding measured in

1163 metabolic cages (n=10 $Cth^{+/+}$ and n=12 $Cth^{-/-}$). Cage image and video show that $Cth^{-/-}$ mice on CysF

1164 diet at day 5 have normal activity. g) Qualitative assessment of nest building (score from 0 to 4)

1165 and presence (score=1) or absence (score=0) of kyphosis in WT and $Cth^{-/-}$ mice (n=12/group). h)

1166 Gait assessment, ledge test and hindlimb clasping test were performed to measure motor

1167 coordination in WT and $Cth^{-/-}$ mice. Mice were scored from 0 (normal behavior) to 1 (abnormal

1168 behavior) (n=12/group). i) Representative H&E-stained sections of kidney, lung, heart, and liver

1169 from female CTH$^{-/-}$ mice fed control diet or Cystine-deficient diet for 6 days, lack significant

1170 pathologic changes and do not differ in microscopic changes by diet in the tissues examined. C =

1171 renal cortex, M = renal medulla A = airway, P = pulmonary artery, > = central vein, and * = portal

1172 triad. Kidney scale bars=200 μm, lung, heart, liver scale bars= 100μm. j) Serum L-methionine, L-

1173 homocysteine, glutamic acid and k) SFAT GSH quantified by mass spectrometry in $Cth^{-/-}$ mice fed

1174 with CTRL or CysF diet for 6 days (n=4-5/group). AU: arbitrary units. l) RNA-seq-based $Nfs1$ and

1175   *Isca1* gene expression in SFAT of *Cth*^{+/+} and *Cth*^{-/-} mice after 6 days of CTRL or CysF feeding

1176   (n=4/group). m) Representative EPR spectra of POBN-lipid radical adducts measured in Folch

1177   extracts of VFAT, SFAT and BAT tissues. The six-line spectrum (red arrows) is consistent with

1178   carbon-centered lipid-derived radicals, indicative of lipid peroxidation (identified through

1179   hyperfine coupling constants $a^N = 15.75 \pm 0.06$ G and $a_\beta^H = 2.77 \pm 0.07$ G). Data are expressed as

1180   mean±SEM. Statistical differences were calculated by 2-way ANOVA with Sidak's correction for

1181   multiple comparisons, or by unpaired t-test (**p<0.01, ***p<0.001).

Extended Data Figure 2, Lee et al
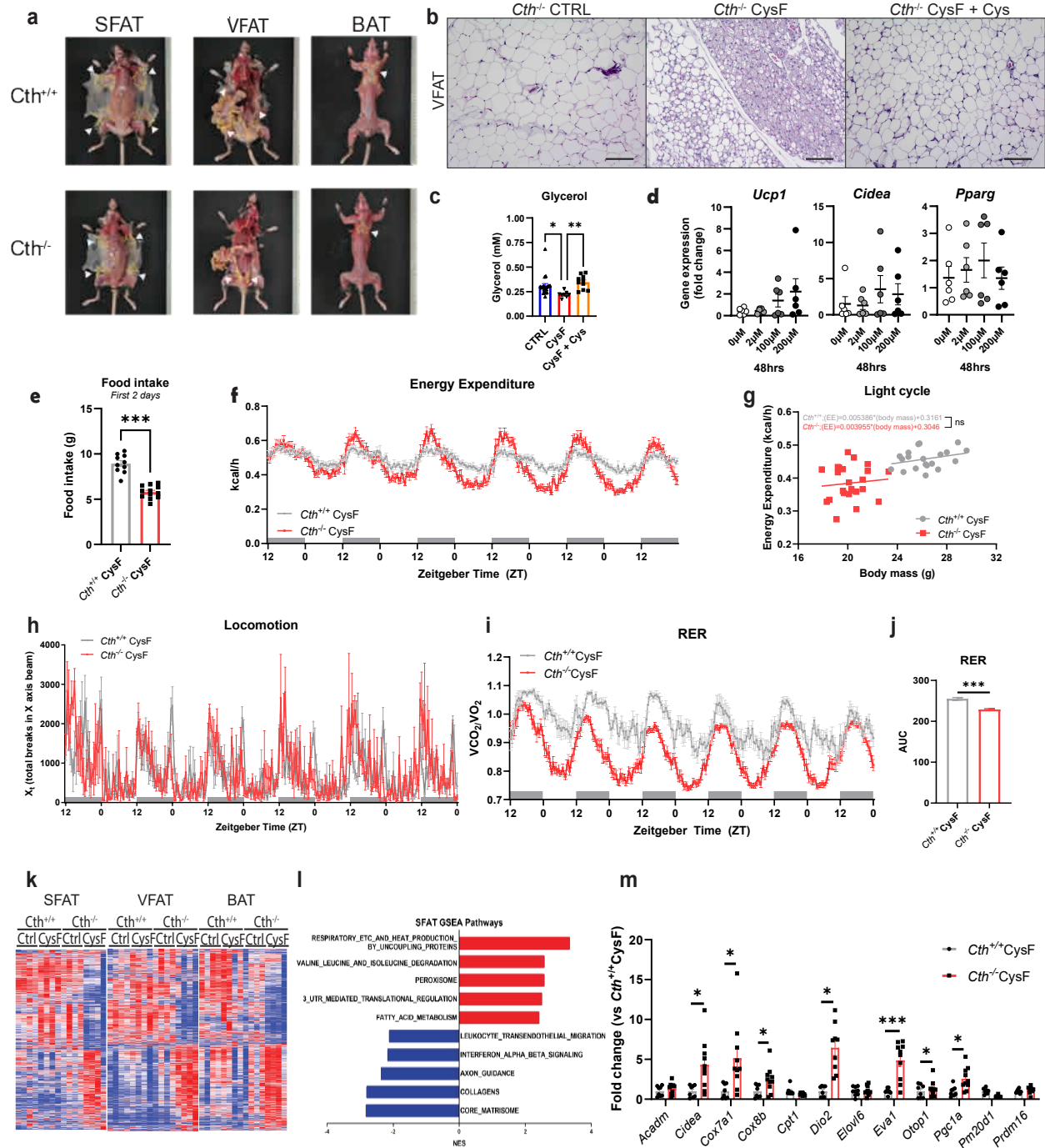
1183 **Extended Data Figure 2: Cysteine starvation induces thermogenic reprogramming of**

1184 **adipose tissue transcriptome**. a) Representative subcutaneous (SFAT), visceral (VFAT), and

1185 brown adipose depots (BAT) of *Cth*^{+/+} and *Cth*^{-/-} after 6 days of CysF diet. b) Representative H&E-

1186 stained sections of VFAT of *Cth*^{-/-} mice fed CTRL or CysF diet for 6 days or after Cys

1187 supplementation following CysF weight loss (scale bar=100 μm). c) Serum glycerol levels of *Cth*[-]

1188 [/-] mice fed with CTRL (n=20) or CysF (n=8) or switched to Cys-containing diet after CysF feeding

1189 (n=10). d) *Ucp1*, *Cidea* and *Pparg* gene expression in *Cth*^{-/-} pre-adipocytes differentiated *in vitro*

1190 and treated with increasing concentration of Cystine for 48 hours. e) Cumulative food intake during

1191 the initial two days of CysF feeding in *Cth*^{+/+} and *Cth*^{-/-} mice (n=10 *Cth*^{+/+} and n=12 *Cth*^{-/-}). f-j)

1192 *Cth*^{+/+} and *Cth*^{-/-} mice were fed with CysF diet for 6 days and housed in metabolic cages (n=10

1193 *Cth*^{+/+} and n=12 *Cth*^{-/-}). f) Energy expenditure during CysF feeding. g) Linear regression analysis

1194 of unnormalized average energy expenditure measured by indirect calorimetry against body mass

1195 on days 4 and 5 of CysF diet. h) Locomotor activity. i) Respiratory exchange ratio (RER) and j)

1196 area under the curve (AUC) quantified for RER. k-l) Whole tissue RNA-seq of SFAT, VFAT, and

1197 BAT of *Cth*^{+/+} and *Cth*^{-/-} fed 6 days of CTRL or CysF diet (n=4/group). k) Heat map highlighting

1198 changes specifically occurring in cysteine deficiency. l) Select top pathways being up- and down-

1199 regulated in *Cth*^{-/-} CysF vs CTRL in SFAT after gene set enrichment analysis. i) Gene expression

1200 of selected thermogenesis markers confirmed by qPCR in SFAT, in *Cth*^{+/+} and *Cth*^{-/-} mice fed with

1201 CysF diet (n=8 *Cth*^{+/+} and n=10 *Cth*^{-/-}. Data are expressed as mean±SEM. Statistical differences

1202 were calculated by one-way ANOVA, or by 2-way ANOVA with Sidak's correction for multiple

1203 comparisons, or by unpaired t-test, (*p<0.05, **p<0.01, ***p<0.001).

1204 *Extended Data Figure 3, Lee et al*

57

1205 **Extended Data Figure 3: Impact of cysteine depletion on transcriptional regulation of**

1206 **adipose tissue at single cell resolution**. a) Experimental design schematic of cell processing of

1207 subcutaneous adipose depot (SFAT) stromal vascular fraction (SVF) for scRNA-seq. b) t-SNE plot

1208 of scRNAseq from SFAT stromal vascular fraction with c) cluster identities. APCs: antigen

1209 presenting cells. ASCs: adipose-derived stromal cells. d) Heat map of normalized gene expression

1210 of selected markers to identify major cell lineages. e) Enrichment of CL-316,243 activated gene

1211 signature overlaid on all populations in all samples. f) t-SNE plots displaying *Dpp4*, *Cd9*, *Icam1*,

1212 *Col5a3*, *F3*, and *Tagln* expression in red across all populations in *Cth*^{-/-} CTRL and *Cth*^{-/-} CysF

1213 samples. g) Volcano plot of differentially expressed genes comparing *Cth*^{-/-} CysF and *Cth*^{+/+} CysF

1214 in cluster 1. h) Orthogonal validation of adipocyte progenitor changes using FACS analysis of

1215 SFAT SVF in *Cth*^{+/+} and *Cth*^{-/-} mice on CTRL and CysF diet for 4 days (n=5-6/group). i) Select

1216 top pathways from gene set enrichment comparing *Cth*^{-/-} CysF vs. *Cth*^{+/+} CysF in cluster 1. j)

1217 Heatmap of gene expression of select stem and mature adipocyte genes in clusters 0, 1 and 2

1218 showing the impact of cysteine depletion in mice. Data are expressed as mean±SEM. Statistical

1219 differences were calculated by 2-way ANOVA with Sidak's correction for multiple comparisons,

1220 and by unpaired t-test (*p<0.05, **p<0.01, ***p<0.001).
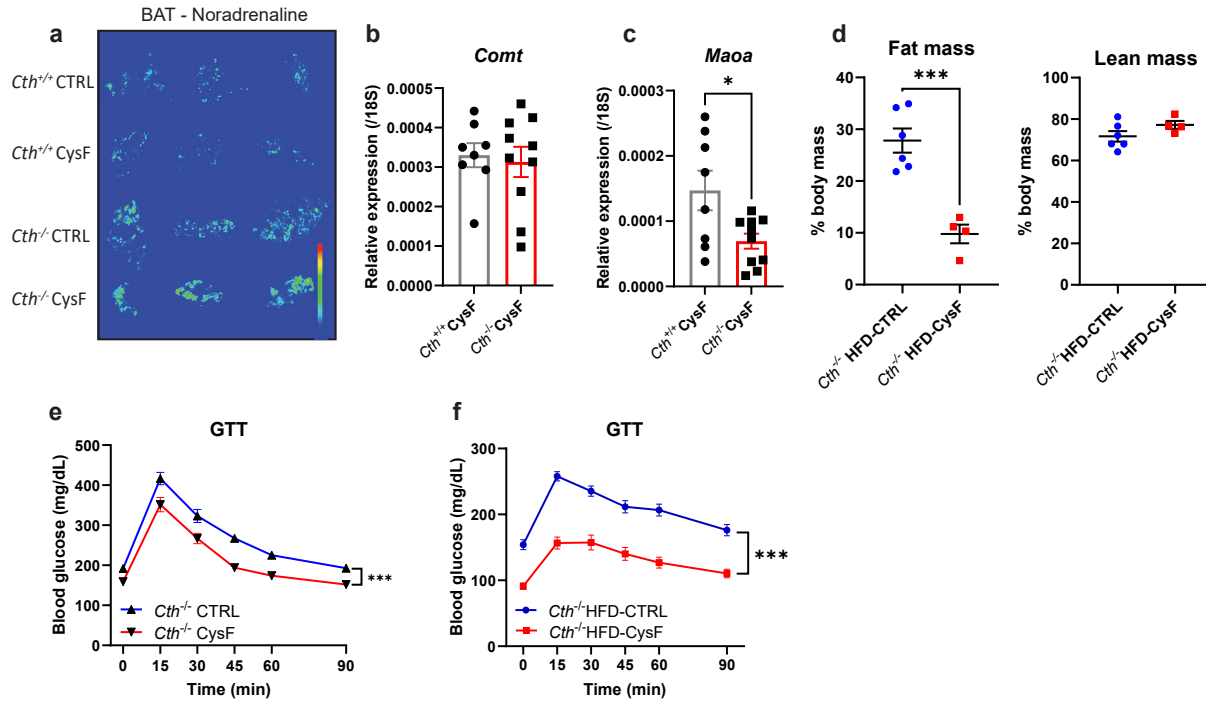
Extended Data Figure 4, Lee et al

Extended Data Figure 4: Cysteine-depletion mobilizes lipids for thermogenic response independently of thermoneutrality. a) Quantification of ATGL immunoblot shown in Fig. 3a, Actin was used as a loading control. b-c) Tissue lipidomics of brown adipose depot (BAT) from $Cth^{-/-}$ mice fed CTRL (n=4) or CysF diet (n=5) for 6 days with b) triglycerides (TG) and c)

59

1226 diacylglycerol species highlighted. AU: arbitrary units. d) Core body temperature (CBT) measured

1227 in the peritoneal cavity by implantation of Star-Oddi logger of $Cth^{-/-}$ mice fed with CTRL or CysF

1228 diet over 6 days and e) average day and night CBT of $Cth^{-/-}$ mice fed with CTRL or CysF diet.

1229 Recordings were taken every 30 minutes (n=11 $Cth^{-/-}$ CTRL, n=12 $Cth^{-/-}$ CysF, 3 independent

1230 experiments pooled). f) $Fgf21$ gene expression in the liver of $Cth^{+/+}$ and $Cth^{-/-}$ mice fed CTRL or

1231 CysF diet for 6 days (n=8 $Cth^{+/+}$ CTRL, n=10 $Cth^{+/+}$ CysF, n=8 $Cth^{-/-}$ CTRL, n=12 $Cth^{-/-}$ CysF). g-

1232 h) Serum levels of g) FGF21 and h) GDF15 in $Cth^{-/-}$ and $Cth^{-/-}$CHOP$^{-/-}$ mice after 5 days of CysF

1233 feeding, measured by ELISA (n=9 $Cth^{-/-}$ and n=7 $Cth^{-/-}$CHOP$^{-/-}$). i) SFAT, VFAT and BAT weight

1234 normalized to body weight of $Cth^{-/-}$ and $Fgf21^{-/-}Cth^{-/-}$ mice after CysF feeding (n=5/group). j)

1235 Respiratory exchange ratio (RER) of $Cth^{-/-}$ and $Fgf21^{-/-}Cth^{-/-}$ mice upon CysF feeding, measured at

1236 day 3 and 4 in metabolic cages (n=5/group). k) $Ucp1$ gene expression in SFAT of $Cth^{-/-}$ and $Fgf21^{-}$

1237 $^{/-}Cth^{-/-}$ mice after 6 days of CysF feeding (n=11-12/group).l) Representative H&E histology images

1238 of SFAT showing increased browning at day 6 in $Cth^{+/+}$ and $Cth^{-/-}$ mice fed CysF diet and housed

1239 at 20°C or at 30°C. m) $Ucp1$ gene expression measured by qPCR in BAT of $Cth^{+/+}$ and $Cth^{-/-}$ mice

1240 fed CysF diet and housed at 20°C or at 30°C for 6 days (n=3-5/group). Data are expressed as

1241 mean±SEM. Statistical differences were calculated by 2-way ANOVA with Sidak's correction for

1242 multiple comparisons, and by unpaired t-test (*p<0.05, **p<0.01, ***p<0.001).

Extended Data Figure 5, Lee et al
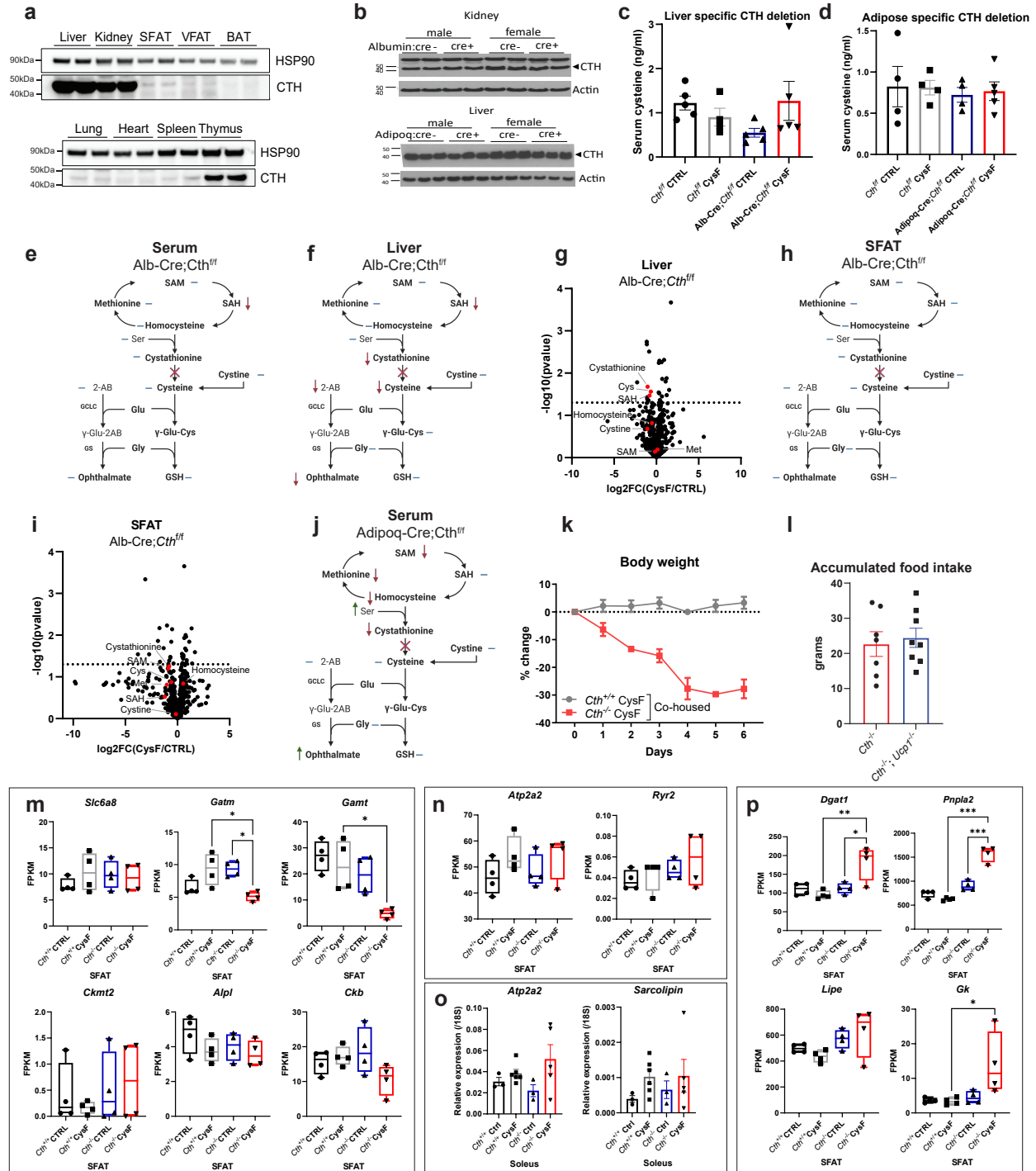
1244 **Extended Data Figure 5: Systemic cysteine depletion induced weight-loss is independent of**

1245 **microbiota and canonical thermogenic pathways.** a) Immunoblot analysis of CTH in liver,

1246 kidney, subcutaneous (SFAT), visceral (VFAT), brown (BAT) adipose depots, lung, heart, spleen,

1247 and thymus. b) Immunoblot analysis of CTH in kidney samples from male and female $Cth^{f/f}$;Alb-

1248 Cre- and $Cth^{f/f}$;Alb-Cre+ mice and in liver samples from male and female $Cth^{f/f}$;Adipoq-Cre- and

1249 $Cth^{f/f}$;Adipoq-Cre+ mice. Actin is used as a loading control. c-d) Cysteine serum levels of c) $Cth^{f/f}$

1250 and Alb-Cre;$Cth^{f/f}$ mice and d) $Cth^{f/f}$ and Adipoq-Cre;$Cth^{f/f}$ mice after 5 days of CTRL or CysF

1251 diet (n=4-5/group). e-i) Alb-Cre;$Cth^{f/f}$ mice were fed CTRL or CysF diet for 6 days. Schematic

1252 summary of changes in the metabolites in the e) serum and in the f) liver. g) Volcano plot of

1253 metabolites identified by MS/MS in the liver. h) Schematic summary of changes in the metabolites

1254 and i) volcano plot of metabolites identified by MS/MS in the SFAT. Transsulfuration pathway

1255 related metabolites are highlighted in red. Cys: cysteine. Met: methionine. SAM: S-adenosyl

1256 methionine. SAH: S-adenosyl homocysteine. j) Schematic summary of changes in serum

1257 metabolites of Adipoq-Cre;$Cth^{f/f}$ fed with CTRL or CysF diet for 6 days. Blue lines represent

1258 measured, but unchanged metabolites, red and green arrows indicate significantly decreased or

1259 increased metabolites, respectively (p<0.05). k) Percentage body weight change of $Cth^{+/+}$ and Cth^{-}

1260 $^{/-}$ mice that were co-housed and fed CysF diet for 6 days (n=4/group). l) Accumulated food intake

1261 of $Cth^{-/-}$ and $Cth^{-/-}$ $Ucp1^{-/-}$ mice during 6 days of CysF diet (n=7 $Cth^{-/-}$ and n=8 $Cth^{-/-}$ $Ucp1^{-/-}$). m-n)

1262 RNA-seq based expression of genes associated with m) creatine futile cycle (*Slc6a8*, *Gatm*, *Gamt*,

1263 *Ckmt2*, *Alpl* and *Ckb*) and n) calcium futile cycle (*Atp2a2* and *Ryr2*) in the SFAT of $Cth^{+/+}$ and Cth^{-}

1264 $^{/-}$ mice fed CTRL or CysF diet for 6 days (n=4/group). o) qPCR gene expression of *Sarcolipin* and

1265 *Atp2a2* in the soleus of $Cth^{+/+}$ and $Cth^{-/-}$ mice fed CTRL or CysF diet for 6 days (n=3 $Cth^{+/+}$CTRL,

1266 n=6 $Cth^{+/+}$CysF, n=3 $Cth^{+/+}$CTRL and n=5 $Cth^{+/+}$CysF). p) RNA-seq based expression of genes

1267 associated with triglyceride and fatty acid metabolism (*Dgat1*, *Pnpla2*, *Lipe*, *Gk*) in the SFAT of

1268 *Cth⁺/⁺* and *Cth⁻/⁻* mice fed CTRL or CysF diet for 6 days (n=4/group). Data are expressed as

1269 mean±SEM. Statistical differences were calculated by 2-way ANOVA with Sidak's correction for

1270 multiple comparisons, and by unpaired t-test (*p<0.05, **p<0.01, ***p<0.001).

1271 *Extended Data Figure 6, Lee et al*

1272 **Extended Data Figure 6: Cysteine starvation induced browning requires adrenergic**

1273 **signaling.** a) Imaging mass spectrometry of noradrenaline in the BAT of *Cth⁺/⁺* and *Cth⁻/⁻* fed 6

1274 days of CTRL or CysF diet. b-c) qPCR gene expression of b) *Maoa* and c) *Comt* in SFAT of *Cth⁺/⁺*

1275 (n=8) and *Cth⁻/⁻* (n=10) mice fed with CysF diet for 6 days. d) Body composition measured by

1276 Echo-MRI on day 6 post diet switch (n=6 *Cth⁻/⁻* HFD-CTRL and n=4 *Cth⁻/⁻* HFD-CysF). e) The

1277 glucose tolerance test (GTT) in mice fed control and cysF diet with glucose dose based on lean

1278 mass. f) The GTT in *Cth⁻/⁻* after diet switch from HFD-CTRL to HFD-CysF (*Cth⁻/⁻* HFD-CTRL

1279 n=19, *Cth⁻/⁻* HFD-CysF, n=20). The glucose administration based on total body-weight. Data are

1280   expressed as mean±SEM. Statistical differences were calculated by 2-way ANOVA with Sidak's

1281   correction for multiple comparisons, and by unpaired t-test (*p<0.05, ***p<0.001).